The receptor-like cytoplasmic kinase MAZZA and CLAVATA-family receptors interact *in vivo*, together mediating developmental processes in *Arabidopsis thaliana*

Patrick Blümke, Jenia Schlegel, Sabine Becher, Karine Pinto, Rüdiger Simon*

Institute for Developmental Genetics, Heinrich Heine University, Universitätsstraße 1, 40225 Düsseldorf, Germany

* Corresponding author: ruediger.simon@hhu.de

Abstract

The receptor-like kinases (RLKs) CLAVATA1 (CLV1) and BARELY ANY MERISTEMs (BAM1 – 3) form the CLV-family (CLVf), which perceives peptides of the CLV3/EMBRYO SURROUNDING REGION (ESR)-related (CLE) family within various signaling pathways of *Arabidopsis thaliana*. CLE peptide signaling, which is required for meristem size control, vascular development, or pathogen responses, involves the formation of receptor complexes at the plasma membrane (PM). These complexes comprise RLKs and co-receptors in varying compositions depending on the signaling context and regulate target gene expression, such as *WUSCHEL* (*WUS*). How the CLE signal is transmitted intracellularly after perception at the PM is not known.

Here, we found that the membrane-associated receptor-like cytoplasmic kinase (RLCK) MAZZA (MAZ) MAZ and additional members of the Pti1-like protein family interact *in vivo* with CLVf receptors. MAZ, which is widely expressed throughout the plant, localizes to the PM via posttranslational palmitoylation potentially enabling stimulus-triggered protein re-localization. We identified a role for a CLV1/MAZ signaling module during stomatal and root development, and redundancy could potentially mask other phenotypes of *maz-1* mutants. We propose that RLCKs such as MAZ mediate CLVf signaling in a variety of developmental contexts, paving the way towards understanding the intracellular processes after CLE peptide perception.

Keywords: CLAVATA, RLK, RLCK, Pti1-like family, CLE peptides, plant development

Introduction

Plant communication and sensing of environmental cues rely on the perception of extracellular signaling molecules via PM-localized cell surface receptors. The genome of *Arabidopsis thaliana* encodes more than 400 membrane-spanning RLKs with intracellular kinase domains (KDs) and versatile types of extracellular domains that perceive e.g. phytohormones, pathogen-associated compounds, or small peptides (Shiu and Bleecker, 2003).

Among this heterogenic group of receptors, CLV1 is one of the best-characterized RLKs with key functions in stem cell regulation in the shoot apical meristem (SAM), inflorescence meristems (IMs), floral meristems (FMs), and the (distal) root meristem (RM) (Stahl and Simon, 2012). Together with its close relatives BAM1, BAM2, and BAM3, CLV1 forms the core family of CLV (CLVf) receptors, which perceive CLE peptides at the PM through their leucine-rich repeat (LRR) receptor domains (Shinohara and Matsubayashi, 2015; Hazak et al., 2017). Beyond meristem homeostasis, CLVf receptors and their associated CLE ligands function in various contexts of plant life, e.g. differentiation of xylem and phloem (Fukuda and Hardtke, 2020), response to bacterial infections (Hanemian et al., 2016), cyst nematode parasitism (Guo et al., 2017), and intercellular spreading of small RNAs or virus particles through plasmodesmata (Rosas-Diaz et al., 2018). Functional diversity of CLE perception via CLVf receptors is also reflected by context-specific interaction and cross-regulation with other RLKs or receptor-like proteins (RLPs).

In the shoot meristems the stem cell derived peptide CLV3, founding member of the CLE family, binds to CLV1 to downregulate the stem cell fate repressing transcription factor WUSCHEL (WUS) as part of a negative feedback loop that dynamically regulates the size of the stem cell domain (Mayer et al., 1998; Schoof et al., 2000; Brand et al., 2000). Besides CLV1, the receptor network that contributes to CLV3 perception in the shoot meristems comprises BAM1 – 3 (DeYoung et al., 2006; Deyoung and Clark, 2008), the heteromeric CLV2/CORYNE (CRN) complex (Jeong et al., 1999; Müller et al., 2008; Bleckmann et al., 2010), and the LRR-RLK RECEPTOR PROTEIN KINASE2 (RPK2) (Kinoshita et al., 2010). BAM1 and BAM2, which were also shown to directly bind CLV3 peptide, can functionally replace CLV1 in the SAM and FM. However, in wild type plants their expression is suppressed in the stem cell domain in a CLV3/CLV1-dependent fashion (Shinohara and Matsubayashi, 2015; Nimchuk et al., 2015). The shoot meristem phenotypes of *clv1* and *clv2*/*crn* mutants are additive, suggesting synergistic effects in sensing CLV3 (Kayes and Clark, 1998; Müller et al., 2008). Although the CLV2/CRN heteromer resembles the structure of a typical LRR-RLK, the

heteromer cannot by itself perceive and transmit CLV3 signals (Nimchuk et al., 2011a; Shinohara and Matsubayashi, 2015).

CLVf receptors are also crucial for CLE perception in the RM. Here, CLV1 is restricted to areas distal to the stem cell organizing quiescent center (QC), where it interacts with the non-LRR-RLK ARABIDOPSIS CRINKLY4 (ACR4) to repress columella stem cell (CSC) fate via a CLE40-dependent pathway (Stahl et al., 2009, 2013). *BAM3* is specifically expressed within the proximal RM in the developing phloem cell files. Here, BAM3 functions as the receptor for CLE45 to regulate sieve element (SE) differentiation together with other phloem-specific factors and the CLV2/CRN heteromer (Anne and Hardtke, 2018; Breda et al., 2019). *BAM1* is broadly expressed in the RM and perceives CLE9/10 peptides to regulate early cell fate decisions during xylem differentiation (Qian et al., 2018).

Co-receptors additionally contribute to the signaling versatility of many LRR-receptor kinase signaling pathways. They are typically characterized by a short extracellular domain with low numbers of LRRs to complete the binding pocket of the corresponding main receptor (recent overview and classification by (Xi et al., 2019)). Mutant analyses and interaction studies revealed that the CLAVATA3 INSENSITIVE RECEPTOR KINASEs1 – 4 (CIK1 – 4) are redundant co-receptors of the CLVf receptors as well as of RPK2 (Hu et al., 2018; Cui et al., 2018; Anne et al., 2018).

The variability of CLVf receptors to function in diverse informational networks with distinct signaling outputs requires mechanisms that add specificity to each pathway. One potential layer of specificity can arise from downstream signaling. However, the immediate early events after recognition of CLE peptides by CLVf receptors are not clear. Studies in maize and Arabidopsis suggest the involvement of heterotrimeric GTP binding protein (G-protein) complexes to integrate CLE peptide responses (Bommert et al., 2013; Ishida et al., 2014; Wu et al., 2020). Mitogen-activated protein kinase (MAPK) cascades, which display a classical mode of intracellular signal transduction in RLK pathways (reviewed in (He et al., 2018)), have been proposed to mediate downstream CLE signaling (Betsuyaku et al., 2011; Lee et al., 2019). However, no physical interaction between CLVf receptors and MAPK signaling elements have yet been shown.

Many cell surface receptor-based signaling pathways rely on RLCKs as key mediators of information transduction, integration, and attenuation (reviewed in (Liang and Zhou, 2018)). RLCKs form a heterogenous group of signaling kinases that are characterized by the absence of extracellular receptor domains and lack a TMD in most cases, however, they can be PM-

associated (Bi et al., 2018). The Arabidopsis genome contains 402 potential *RLCK*-encoding genes that cluster into 15 phylogenic sub-groups (Shiu et al., 2004; Fan et al., 2018). These comprise proteins like the RLCK class VII member BOTRYTIS-INDUCED KINASE1 (BIK1), which acts as an important signaling hub downstream of various LRR-RLKs to control immune responses, e.g. via FLAGELLIN SENSING2 (FLS2), but also mediates processes of developmental regulation through BRASSINOSTEROID INSENSITIVE1 (BRI1) or the ERECTA-family (ERf) (Lu et al., 2010; Lin et al., 2013; Chen et al., 2019). Moreover, non-LRR-RLKs also depend on RLCKs. For example. FERONIA (FER), ANXUR1 (ANX1), or ANX2 from the *Catharanthus roseus* RLK1-like (*Cr*RLK1L) family regulate cell wall (CW) integrity through MARIS (MRI) (Boisson-Dernier et al., 2015). MRI belongs to the RLCK VIII subgroup, which contains 11 Arabidopsis genes that share high sequence similarity with *Pti1* from *Solanum lycopersicum* (tomato), a target of the Pto kinase conferring resistance against the bacterial speck disease (Zhou et al., 1995; Sessa et al., 2000). Furthermore, members of the Pti1-like proteins in Arabidopsis (Pti1-1, Pti1-2, Pti1-3, Pti1-4) were shown to interact with OXIDATIVE STRESS INDUCIBLE1 (OXI1), which mediates the cellular response to stress signals like ROS and fungal elicitors. Pti1-4 was also associated with MAPK signaling downstream of OXI1 (Anthony et al., 2006; Forzani et al., 2011). Additionally, the Pti1-like family members CYTOSOLIC ABA RECEPTOR KINASE1 (CARK1) and CARK6 were found to be interactors of the REGULATORY COMPONENTS OF ABA RECEPTORS (RCARs) that function in perceiving the phytohormone abscisic acid (ABA), a general trigger of abiotic stress responses (Zhang et al., 2018; Wang et al., 2019).

Although some members from the RLCK VIII family in Arabidopsis have emerged as crucial signaling intermediates of several pathways, most Pti1-like homologs are not characterized in detail, or not at all. We here report the identification of MAZZA (MAZ, Pti1-3), a member of the RLCK subgroup VIII, as an interactor of the CLVf receptors, thereby expanding the potential range of the RLCK VIII / Pti1-like family to LRR-RLK pathways. We found that CLV1 and MAZ together are involved in developmental processes within stem cell regulation in the RM and during stomatal patterning.

127 **Results**

128 **MAZ interacts with CLV1 *in vivo***

129 CLVf receptors are critical for meristem homeostasis but also play pivotal roles during other
130 developmental and physiological signaling events. This is, for example, reflected in the
131 expression of *CLV1* in various tissues besides the shoot meristems, like companion cells (CCs)
132 of the phloem in aerial organs and the root, and in the distal RM. Furthermore, we found that
133 *CLV1* is expressed in the epidermis of cotyledons and true leaves, particularly in developing
134 cells of the stomata lineage (Fig. 1, Suppl. Fig. 1 A). However, direct downstream targets of
135 CLVf receptors are not known in any of those tissues. To identify CLV1 interactors we applied
136 an untargeted, non-organ-biased co-immunoprecipitation (CoIP) approach with magnetic anti-
137 GFP beads (ChromoTek) against CLV1-2xGFP from whole Arabidopsis seedlings expressing
138 the receptor-fluorophore fusion under the control of the endogenous *CLV1* promotor. This
139 transgene is fully functional and was previously shown to complement the known phenotypes
140 of *clv1* mutants (Nimchuk et al., 2011b). Via subsequent mass spectroscopy analyses of the Co-
141 IP fractions we detected Pti1-like proteins among the peptide sequences specifically pulled
142 down with CLV1 and not found in GFP controls (Suppl. Tab. 1). Most of those hits were unique
143 for Pti1-3, while some identified peptide sequences also aligned to other Pti1-like members.
144 Among the candidates for CLV1 interaction we identified Pti1-3 as most promising due to its
145 predicted PM-localization and kinase function. The *Pti1-3* gene (At3g59350) encodes a protein
146 with a predicted KD and an undefined N-terminal region. Due to its capability to interact with
147 CLV1 *in vivo* we dubbed the protein MAZZA (MAZ, Italian for "club", in analogy to the Latin
148 "clavata", and Greek "coryne").

149 MAZ is also found in complex with CLV1 when following a targeted CoIP strategy with leaf
150 material from *Nicotiana benthamiana* plants, transiently expressing the respective interaction
151 partners fused either to GFP or mCherry (mCh) to allow subsequent immunodetection (Fig
152 2 A). Supplying CLV3 peptide prior to protein extraction did not influence complex formation
153 with CLV1, pointing towards a constitutive, ligand independent interaction. To analyze the
154 complex at subcellular level, we applied Förster resonance energy transfer (FRET)-based
155 fluorescence-lifetime imaging microscopy (FLIM) and demonstrated direct interaction between
156 MAZ and CLV1 at the PM (Fig. 2 B). In these FLIM experiments within transiently
157 transformed *N. benthamiana* leaf epidermis cells, the donor-lifetime of CLV1-GFP decreases
158 significantly in the presence of MAZ-mCh (mean FRET efficiency of 5.9 %, Supp. Tab. 2),
159 while a PM-located negative control tagged to mCh affects donor lifetime only at a mean FRET
160 efficiency of 2.0 %, which we defined as the background level for randomly distributed acceptor

161 fluorophores in all following FLIM assays. Infiltration of 5 µM CLV3 peptide into the leaves
162 before FLIM measurements did not affect lifetime. This suggests that CLV3 ligand binding to
163 CLV1 neither enhances the interaction with MAZ, nor induces a rapid dissociation of the two
164 proteins within this experimental setup.

165 **MAZ and Pti1-like homologs interact with CLVf receptors and related pathway elements**

166 Next, we extended the FRET-FLIM interaction studies in the *N. benthamiana* expression
167 system to test if MAZ can interact with other proteins that contribute to CLE peptide perception.
168 We detected interactions at the PM between MAZ and the CLVf receptors BAM1 and BAM3
169 with mean FRET efficiencies of 6.5 % and 4.0 %, respectively (Fig 3 A, B, Suppl. Tab. 2).
170 Furthermore, MAZ interacts with the co-receptor CIK2 (5.7 %, Fig 3 A), and with CRN in the
171 presence of CLV2 (3.0 %, Fig. 3 B). These data indicate that MAZ could integrate different
172 CLE peptide triggered RLK pathways.
173 Additionally, lifetime of MAZ-eGFP decreases in the presence of MAZ-mCh with a mean
174 FRET efficiency of 5.3 % (Fig.3 A). Thus, MAZ can form dimers or higher ordered homomers,
175 which might reflect auto-regulative mechanisms.
176 Since all 11 members of the Pti1-like family in Arabidopsis are highly conserved at amino acid
177 (aa) sequence level (Appendix), they might be functionally redundant. Indeed, from four Pti1-
178 like homologs that we tested additionally to MAZ, three, namely CARK1, CARK6, and Pti1-
179 11 were able to interact with CLV1 at the PM of *N. benthamiana* leaf epidermis cells with mean
180 FRET efficiencies ranging from 4.2 to 5.4 %. Only Pti1-2 showed no interaction with CLV1
181 (Fig. 3 C). This observation is not reflected in the phylogeny of the Pti1-like family, because,
182 for example, CARK1 is more distantly related to MAZ than Pti1-2 (Fig. 3 D). However,
183 differences in the phylogeny do not necessarily concern the sequences that are crucial for
184 protein complex formation. *Vice versa*, detecting no change of donor lifetime in the presence
185 of a certain acceptor does not generally exclude physical interaction, e.g. if the fluorophore
186 fusion sterically hinders energy transfer.

187 **Subcellular localization of MAZ at the PM depends on palmitoylation**

188 MAZ interacts with RLKs and other signaling proteins at the PM. Accordingly, all analyzed
189 MAZ fusion proteins with different fluorophores are PM-localized after transgene expression
190 in *N. benthamiana* (Suppl. Fig. 3, 4) as well as in *A. thaliana* (Fig. 4, 5 Suppl. Fig. 1, 6, 7).
191 MAZ co-localization with CLV1 at the PM is not extended to CLV1-GFP vesicles in
192 *N. benthamiana* cells, which indicate receptor sequestration (Suppl. Fig. 3). This suggests that

193 MAZ is not sequestered together with CLV1 but might instead follow distinct signaling routes
194 after RLK activation and turnover.
195 The MAZ protein sequence does not harbor any TMD, but the N-terminal region possesses
196 predicted palmitoylation sites (C48, C49, Suppl. Tab. 3). S-acylation, i.e. covalent binding of
197 palmitic acid or other fatty acids to the thiol group of cysteine residues, is reversible and thus
198 can represent a mechanism of specific regulation (Hurst and Hemsley, 2015). We found that
199 the predicted MAZ palmitoylation sites are responsible for its PM-localization. Exchanging the
200 corresponding cysteines in the fusion construct *MAZ*^{PalMut}*-eGFP* results in high amounts of
201 cytoplasmic fluorescence signals instead of PM-localization of the fusion protein after
202 expression in *N. benthamiana* or Arabidopsis (Fig 4, Suppl. Fig. 4). This strongly indicates that
203 subcellular PM localization of MAZ relies on post-translational modification via S-acylation.

204 ***MAZ* shares expression domains with the CLVf receptors in *A. thaliana***

205 *MAZ* is expressed in various tissues and organs of Arabidopsis including the distinct expression
206 domains of the CLVf receptors. Analyzing several independent fluorescent *MAZ* reporter lines,
207 we observed differences between translational and transcriptional reporters suggesting that the
208 *MAZ* coding sequence may affect protein expression (Suppl. Fig. 5). Thus, in the following
209 experiments we used translational lines comprising the *MAZ* promotor sequence and the *MAZ*
210 coding sequence including introns to study *MAZ* expression.
211 In the shoot, *MAZ* is expressed in cells of the leaf epidermis, including stomata precursor cells
212 and guard cells (GCs), the vasculature, and the hypocotyl epidermis (Fig 5 D, Suppl.
213 Fig. 1, 6 C). Furthermore, within the inflorescence we detected *MAZ* expression in the IM,
214 primordia and FMs. Signal intensity is elevated in the outermost cell layer (L1) with expression
215 peaks at the boundary regions to emerging primordia. Expression appears to be highest in newly
216 formed primordia and slightly attenuates during further development. (Fig. 5 A, Suppl. Fig. 7).
217 Within the root, *MAZ* is expressed in the epidermis, particularly in root hair cells, in the
218 vasculature, and in the RM. *MAZ* is also expressed in emerging lateral roots from early stage
219 onwards. In mature lateral roots expression resembles the pattern in the main root (Fig 5 B, C,
220 Suppl. Fig. 6). *MAZ* expression in the RM is characterized by elevated signal intensities in the
221 QC and the surrounding stem cells. Expression decreases from the initials gradually towards
222 the elongation zone. However, in developing phloem cell files fluorescence signals are not
223 attenuated but continue upstream in the vasculature cylinder (Fig. 5 B, Suppl. Fig. 6). Marking
224 the position of mature SEs by aniline blue staining revealed that *MAZ* expression in the

225 differentiated vasculature is concentrated in CCs and procambial tissue, but barely in the SEs
226 (Suppl. Fig. 1 B, C).
227 We detected *MAZ* signals in all *CLV1* expression domains (compare Fig. 1). Double reporter
228 lines show co-localization of CLV1-GFP and MAZ-mCh, for example, at the border region to
229 emerging primordia in the IM and in the distal RM (Suppl. Fig. 8). Furthermore, *MAZ*
230 expression comprises previously reported expression domains of *BAM1* and *BAM3* (Depuydt
231 et al., 2013; Shimizu et al., 2015). Thus, local distribution of MAZ allows its participation in
232 different CLVf receptor pathways in Arabidopsis.

233 **MAZ mediates CLE peptide signaling in root development**

234 We characterized the functional impact of MAZ within CLVf pathways by analyzing mutants
235 harboring the T-DNA *maz* allele GABI-Kat 485F03, hereafter referred to as *maz-1*. The
236 insertion event disrupts the KD of MAZ before the predicted active site and m*az-1* plants show
237 substantial decrease of full-length *MAZ* transcripts (~30-fold in comparison to wild type
238 samples, Suppl. Fig. 9).
239 Elevated organ number typically associated with *clv*-like phenotypes reflects enhanced stem
240 cell activity in meristems, concomitant with an increase in the sizes of shoot and floral
241 meristems. While *clv3-9*, *clv1-20*, and *crn-10* show increased carpel numbers per silique, *maz-*
242 *1* plants resemble the wild type. The double mutants *clv1-20;maz-1* and *crn-10;maz-1* resemble
243 the single mutants *clv1-20* and *crn-10*, respectively, indicating that a loss of MAZ is insufficient
244 to disrupt CLV3 signaling (Fig. 6 A, Suppl. Fig. 10).
245 To test MAZ function within CLE40-mediated stem cell differentiation in the distal RM, we
246 quantified CSC layers in *maz-1* roots. Both, *cle40* and *clv1* mutants show increased CSC
247 number due to reduced CLE40 signaling (Stahl et al., 2009, 2013). While increased CLE40
248 peptide in the growth medium reduces CSC layers in the wild type, *clv1-20* mutants are
249 desensitized and maintain more CSC layers. *Maz-1* mutants resemble the wild type on standard
250 growth medium but are partially resistant against external CLE40 peptide treatment that causes
251 drastic reduction of CSC layers in Col-0 (Fig. 6 B, Suppl. Fig. 11). Notably, we found that the
252 double mutant *clv1-20;maz-1* is fully sensitive to CLE40 peptide. This could point to an
253 additional, parallel CLE40 perception pathway during CSC specification, for example via
254 BAM1, which is activated in the absence of both CLV1 and MAZ.
255 CLE peptide treatment not only affects CSC fate but also root growth due to premature
256 differentiation of the proximal RM. Disruption of CLE perception, for example, in *clv2, crn*, or
257 *rpk2* mutants confers resistance against CLE-induced root shortening (Fiers et al., 2005;

258 Shimizu et al., 2015; Müller et al., 2008). Here, we accessed root lengths of plants grown on
259 CLV3 peptide, which is not produced in roots but can generally substitute all root-active CLE
260 peptides in terms of root shortening, and CLE45 peptide, which is expressed in developing
261 phloem files and perceived via BAM3 and CRN/CLV2 (Hazak et al., 2017). Our root growth
262 assays revealed that *maz-1* single mutants are less sensitive than Col-0 seedlings to
263 physiological concentrations of either CLV3 or CLE45 peptide. However, *maz-1* plants grown
264 in the presence of 100 nM CLE peptides display root reductions comparable to wild type
265 samples (Fig. 6 C). We also observed that the *maz-1* allele partially antagonizes *crn-10*
266 mediated resistance to CLV3 peptide in *crn-10;maz-1* double mutants at 10 nM peptide
267 concentration. Similar to the proposed role in CSC fate control, this could again indicate a dual
268 function of MAZ to mediate CLE responses and simultaneously repressing parallel acting CLE
269 perception pathways.
270 Together, our data suggest that MAZ is involved in several CLE signaling pathways, involving
271 CLV1 and CLV2/CRN.

272 We also accessed morphology and physiological constraints of *maz-1* plants regarding
273 previously described phenotypes of other *pti1-like* mutants, i.e. impaired root hair development
274 of *mri* mutants (Boisson-Dernier et al., 2015), and hypersensitivity to drought stress like *cark1*
275 and *cark6* mutants (Zhang et al., 2018; Wang et al., 2019). However, in contrast to *mri-2* and
276 *fer-4* mutants, *maz-1* seedlings display mean root hair length at wild type-level (Suppl. Fig. 12).
277 Furthermore, within two different experimental setups, neither *maz-1* mutants nor *MAZ*
278 overexpression lines show altered drought stress responses, which have been associated with
279 disturbed ABA signaling of mutants or overexpressors of *CARK1* and *CARK6*, respectively
280 (Suppl. Fig. 13, 14).

281 **A novel role for CLV1 with MAZ in stomatal spacing**

282 Regular patterning of stomata at the leaf epidermis is the result of finely controlled series of
283 cell divisions of the stomata cell lineage. In this process meristemoid mother cells (MMCs)
284 divide asymmetrically to form a meristemoid and a larger sister cell. While meristemoids are
285 precursors of guard mother cells (GMCs) that differentiate into the two GCs of a stoma, the
286 sister cell may become a pavement cell or undergoes a spacing division before generating a new
287 meristemoid (reviewed in (Bergmann and Sack, 2007)). Mutants lacking this regular spacing
288 between two stomata, for example, due to disruption of the receptor complex that senses
289 positional cues in the leaf epidermis, include, among others, *er;erecta-like1(erl1);erl2* triple
290 mutants of the *ERf* receptor genes and mutants of the LRR-RLP encoding *TOO MANY*

291 *MOUTHS* (*TMM*) gene. These mutants accumulate two or more stomata directly adjacent to
292 each other, i.e. display stomatal clustering (reviewed in (Zoulias et al., 2018)).
293 We observed that *clv1* mutants are also associated with defects in regular patterning in the leaf
294 epidermis (Suppl. Fig. 15). Initial data revealed an increased number of stomata in true leaves,
295 but not in cotyledons, of *clv1-20* plants in comparison to wild type Col-0, uncovering a novel
296 role for CLV1 in stomatal patterning. Furthermore, CLE peptide treatment antagonized this
297 effect in *clv1-20* mutants (Suppl. Fig. 15). We extended these analyses to include *maz-1* and
298 the double mutant *clv1-20;maz-1*. Quantification of stomatal clusters in seedlings 14 DAG
299 grown on ½ MS agar plates, not only confirmed defects in patterning of *clv1-20* true leaves, but
300 also showed that the double mutant *clv1-20;maz-1* enhances this phenotype (Fig. 7). In
301 comparison to the wild type control (Col-0) the mean stomata cluster rate of *clv1-20* is elevated
302 (~ 2 % stomata in cluster). However, in *clv1-20;maz-1* cluster rate is significantly increased to
303 ~ 10 %, while the single *maz-1* mutant displays no clusters. Stomata density was not
304 significantly different between genotypes. This points towards a specific function of CLV1 and
305 MAZ in spacing divisions, but not stomata specification. Since both, *MAZ* and *CLV1*, are
306 expressed in cells of the stomatal lineage (Fig. 1 E, 5 D), we propose that the CLV1/MAZ
307 signaling module serves to establish stomata spacing.

308 **Discussion**

309 CLVf RLKs participate in various signaling systems, thereby controlling meristem homeostasis
310 but also processes like vascular formation or plant immunity. Here, we add stomata
311 development to the scope of CLV1 functions. Considering the diversity of CLVf pathways,
312 mechanisms to mediate specific downstream responses are required. In their role as direct
313 interactors of CLVf receptors, MAZ and several of its homologs are prime candidates to
314 participate in downstream signaling after CLE perception. Furthermore, the expression pattern
315 of *MAZ* overlaps with the places of action of the CLVf receptors in Arabidopsis. Therefore,
316 MAZ might integrate and cross-regulate signaling cues from different CLVf receptors.

317 **Functional redundancy of Pti1-like homologs could mask mutant phenotypes**

318 We found that *maz-1* plants are resistant to exogenous CLE treatment in the context of CSC
319 specification (Fig. 6 B). However, in comparison to *clv1-20* mutants, the resistance of *maz-1* is
320 less pronounced. Also, the CLE peptide resistance of *maz-1* seedlings regarding proximal RM
321 development is less penetrating than in mutants of the involved receptors. At higher CLE
322 peptide concentrations root shortening of *maz-1* seedlings resembles the level of wild type-
323 samples (Fig. 6 C). Furthermore, the *maz-1* allele confers no *clv1*-like increased carpel number
324 (Fig. 6 A). These observations suggest that other Pti1-like homologs compensate MAZ function
325 in *maz-1* mutants. In line, several Pti1-like proteins interact with CLV1, reflecting a conserved
326 binding capacity of Pti1-like homologs to the CLVf receptors (Fig. 3 C).
327 Functional redundancy is a common feature within the Pti1-like family. For example, Pti1-1,
328 Pti1-2, and Pti1-3 (=MAZ), respectively, interact with the stress-related kinase OXI1 (shown
329 by yeast-two-hybrid and Co-IP). However, only the interaction of OXI1 with Pti1-2 was
330 validated by stimulus triggered phosphorylation *in vivo* (Anthony et al., 2006). This indicates a
331 high general potential of functional redundancy but at the same time demonstrates the presence
332 of mechanisms that add specificity to the respective Pti1-like homologs within their
333 physiological context.

334 **The N-terminus of Pti1-like proteins could determine functional specification**

335 The 11 Pti1-like homologs in Arabidopsis are especially conserved within the KDs, while their
336 more variable N-termini allow specification (Appendix). As we demonstrated in here, the MAZ
337 N-terminus determines its subcellular localization via palmitoylation (Fig. 4). In contrast to
338 other mechanisms that mediate PM-localization, the attachment of a palmityl group via S-
339 acylation is reversible. As such, palmitoylation can dynamically regulate the subcellular

340 localization of proteins (reviewed in (Hurst and Hemsley, 2015)). All Pti1-like family members
341 in Arabidopsis, except Pti1-6, harbor conserved cysteines, which are predicted palmitoylation
342 sites (Suppl. Tab. 3). In general, S-acylation is often coincidently found with protein
343 myristoylation. However, within the Arabidopsis Pti1-like family only CARK1 is additionally
344 equipped with a myristoylation site, suggesting it is obligatorily PM-localized. The subcellular
345 localization of the other nine Pti1 homologs in Arabidopsis might be dynamically controlled by
346 counteracting protein S-acyl transferases (PATs) and acyl protein thioesterases. Although the
347 underlying mechanisms in plants are not well understood (reviewed in (Li and Qi, 2017)),
348 palmitoylation allows stimulus-triggered subcellular re-localization and display a powerful tool
349 for signal transduction. S-acylation of Pti1-like proteins is evolutionary conserved among
350 various species, including monocots, as shown e.g. for ZmPti1a from maize and OsPti1a from
351 rice (Herrmann et al., 2006; Matsui et al., 2014).
352 Notably, the MAZ N-terminus is longer than in most of its Arabidopsis homologs, potentially
353 offering additional target sites for specific control, such as differential phosphorylation or
354 protein turnover via ubiquitination. It comprises two Phospho-Serines (detected in the
355 PhosphAt Database (Heazlewood et al., 2008)) and according to different prediction tools 3 –
356 7 lysine residues as potential targets for ubiquitination.

357 **CLV1/MAZ contributes to spacing divisions in stomata development**

358 Feedback-regulated signaling systems are crucial to integrate positional information from
359 neighboring cells or tissues into developmental processes and to ensure dynamic but controlled
360 growth. Such feedback loops determine, for instance, the stem cell domain in the SAM, IMs,
361 and FMs (Fletcher et al., 1999; Brand et al., 2000), and cell fate in the leaf epidermis during
362 stomatal patterning (reviewed in (Tameshige et al., 2017)). While the CLV pathway is the major
363 regulative element in the shoot meristems, the ERf receptors are essential for cell fate decisions
364 during leaf epidermis differentiation. However, the ERf also impacts stem cell homeostasis in
365 the shoot meristems (Uchida et al., 2013; Mandel et al., 2014; Zhang et al., 2020). In turn, CLV-
366 related pathways are involved in stomatal development, e.g. by perceiving CLE9/10 peptides
367 (Qian et al., 2018). In here we provide first evidences that *clv1-20* mutants are defective in
368 regular patterning of GCs and that *maz-1* enhances this phenotype as a second site mutation
369 (Fig. 7).
370 In the epidermis of cotyledons and true leaves the *CLV1* promotor is predominantly active in
371 meristemoids and stomatal lineage ground cells, while *CLV1* expression is barely detectable in
372 differentiated epidermis cells, neither in pavement cells nor in GCs (Fig. 1). This hints toward

373 a specific function of the CLV1 receptor within the precise signaling events of leaf epidermis
374 differentiation. The notion that *clv1* mutants, in contrast to, for example, *tmm* mutants (Geisler
375 et al., 2000), show rather mild stomatal patterning defects suggests the presence of redundantly
376 acting genes. Furthermore, stomata density in *clv1* mutants is comparable to the wild type (Fig.
377 7). Thus, CLV1 does not determine MMC fate, but may act later in the stomatal lineage to
378 establish the one-cell-spacing rule between two stomata. This stomatal spacing is mainly
379 regulated by EPIDERMAL PATTERNING FACTOR 1 (EPF1) and its primary receptor ERL1,
380 which form a negative feedback loop with the transcription factor MUTE (Hara et al., 2007;
381 Lee et al., 2012; Qi et al., 2017). CLV1-based signaling could interfere with this feedback
382 regulation or act in parallel to finetune spacing divisions.
383 Our observation that the double mutant *clv1-20;maz-1* displays increased stomata cluster rate
384 in comparison to *clv1-20* single mutants (Fig. 7) suggests that MAZ is not only involved in
385 stomatal pattering as a potential downstream target of CLV1, but also affects spacing divisions
386 through CLV1-independent signaling. Therefore, MAZ is possibly a shared downstream target
387 of CLV1 and other RLKs, e.g. ERL1. Since *maz-1* single mutants are wild type-like regarding
388 stomata clusters, redundancy mediated by other Pti1-like homologs can be assumed. However,
389 in combination with the *clv1-20* mutation this redundancy is partly overcome. This might be
390 explained by the quantitative character of CLV1/MAZ signaling during stomatal development
391 comprising additional, yet unknown components.

392 **Conclusions**

393 We here report on the identification of MAZ and other RLCKs of the Pti1-like family as
394 intermediators of CLVf receptor responses. Within the versatile functional contexts of CLVf
395 pathways, MAZ and redundantly acting homologs could contribute to differential signaling
396 outputs. After CLE perception by CLVf receptors, signal transduction may involve
397 transphosphorylation between the CLVf RLKs and Pti1-like RLCKs and subsequent
398 detachment of MAZ or its homologs from the membrane to reach intracellular targets (compare
399 Fig. 8). Deciphering how MAZ and the CLVf are functionally connected will be critical for
400 further characterization of the Pti1-like family as downstream elements of CLVf receptor
401 pathways.

402 **Material and Methods**

403 Detailed information on chemicals used for the described experiments are available in Suppl.
404 Tab. 4.

405 **Plant material and growth conditions**

406 All *Arabidopsis thaliana* (L.) Heynh. plants in this study are ecotype Columbia-0 (Col-0).
407 Origin and details on utilized mutants harboring the alleles *maz-1*, *clv1-20*, *crn-10*, *clv3-9*,
408 *cark1-2*, *cark6-1*, *mri-2*, and *fer-4*, respectively, can be found in Suppl. Tab. 5. The presence of
409 the respective alleles was controlled following genotyping strategies as listed in Suppl. Tab. 6.
410 Before sowing, *A. thaliana* seeds were sterilized in ethanol solution (10 min in 80 % v/v ethanol,
411 1.3 % w/v sodium hypochlorite, 0.02 % w/v SDS), or in a chloric gas atmosphere (1 h in a
412 desiccator after mixing 50 ml of 13 % w/v sodium hypochlorite with 1 ml 37 % HCl,). If not
413 indicated differently, plants were cultivated in phytochambers under long day (LD) conditions
414 (16 h light / 8 h dark) at 21 °C on soil. Alternatively, seedlings were cultivated for up to 14 days
415 on ½ MS agar plates (1 % w/v sucrose, 0.22 % w/v MS salts + B5 vitamins, 0.05 % w/v MES,
416 12 g/l plant agar, adjusted to pH 5.7 with KOH) in phytocabinets (continuous light, 60 %
417 humidity, and 21 °C).
418 *N. benthamiana* plants were grown 4 – 5 weeks in the greenhouse and subsequently used for
419 transient leaf epidermis cell transformation. After infiltration, *N. benthamiana* plants were kept
420 under high humidity in continuous light.

421 **Cloning**

422 Information on the entry plasmids, subsequently used for the assembly of plant expression
423 vectors can be found in Suppl. Tab. 7. New entry plasmids generated in this study contain DNA
424 sequences that were PCR-amplified (with Phusion High-Fidelity PCR polymerase) from
425 genomic DNA prepared of Col-0 rosette leaves. PCR fragments were introduced via customized
426 oligonucleotide overhangs to either pENTR® (Gateway® system, (Katzen, 2007)) or pGGA000
427 and pGGC000 (GreenGate system, (Lampropoulos et al., 2013)). Coding sequences of genes
428 of interest (GOIs) were amplified without the STOP codon to allow C-terminal fusions with
429 fluorophores. Single positions within gene sequences were modified by site-directed
430 mutagenesis applying the QuikChange II kit according to manufacturer's protocol (Agilent
431 Technologies).
432 Destination plasmids utilized for transient expression in *N. benthamiana* and for generation of
433 stable *A. thaliana* lines are listed in Suppl. Tab. 8 and 9, respectively. Inducible vectors were

434 created by a Gateway® LR reaction (according to manufacturer's instructions, Thermo Fisher
435 Scientific), combining an entry vector harboring the GOI with either pABindGFP or
436 pABindmCherry (Bleckmann et al., 2010). Transgenes for constitutive *N. benthamiana* and
437 stable Arabidopsis expression were constructed with the GreenGate system, assembling desired
438 DNA sequences and the backbone pGGZ001 following a golden gate principle (compare Suppl.
439 Tab. 8 and 9).
440 To amplify plasmid DNA, competent *Escherichia coli* DH5α cells were heat-shock transformed
441 and cultivated on selective LB medium (1 % w/v tryptone, 0.5 % w/v yeast extract, 0.5 % w/v
442 NaCl). After plasmid DNA purification via commercial kits, the plasmids were validated by
443 restriction digest and Sanger sequencing.

444 **Transient gene expression in *N. benthamiana***

445 Agrobacterium-mediated transformation of leaf epidermis cells of *N. benthamiana* was applied
446 to monitor transient expression of transgenes. The *Agrobacterium tumefaciens* strain GV3101
447 pMP90 (rifampicin and gentamycin resistant) was used. Bacteria were transformed with the
448 required plasmid vectors via the heat-shock method (aliquots of competent cells mixed with 1
449 µl 100 nM plasmid DNA were incubated for 5 min in liquid N_2 followed by 5 min at 37 °C and
450 subsequent regeneration). All Gateway®-based destination plasmids were introduced to
451 GV3101 pMP90 additionally equipped with an expression cassette for the p19 suppressor of
452 gene silencing from the tomato bushy stunt virus to enhance efficiency of transgene expression
453 (Voinnet et al., 2003). Plasmids constructed via the GreenGate system were introduced to *A.*
454 *tumefaciens* GV3101 pMP90 pSoup. The helper plasmid pSoup confers resistance against
455 tetracycline and contains the *RepA* gene, which encodes a trans-activating replicase for the pSA
456 origin of replication that is mandatory for propagation of GreenGate-based destination plasmids
457 in *A. tumefaciens* (Hellens et al., 2000).
458 For infiltration of *N. benthamiana* leaves, agrobacteria containing the respective expression
459 cassettes were cultivated overnight with shaking at 28 °C in 5 ml dYT (double Yeast Tryptone,
460 1.6 % w/v tryptone, 1 % w/v yeast extract, 0.5 % w/v NaCl) with appropriate antibiotics
461 (Gateway® plasmids in GV3101 pMP90 p19 with 50 µg mL^{-1} rifampicin, 50 µg mL^{-1}
462 gentamycin, 50 µg kanamycin, and 100 µg mL^{-1} spectinomycin; GreenGate plasmids in
463 GV3101 pMP90 pSoup with 50 µg mL^{-1} rifampicin, 50 µg mL^{-1} gentamycin, 2.5 µg
464 tetracycline, and 100 µg mL^{-1} spectinomycin). Cell cultures were adjusted to an optical density
465 (OD_{600nm}) of 0.3 and centrifuged (10 min, 4000 x g, 4 °C). The pellet was resuspended in
466 infiltration medium (5 % w/v sucrose, 150 µM acetosyringone, 0.01 % v/v Silwet) and

467 incubated at 4 °C for 2 – 3 h. For co-expression of two or more transgenes, the corresponding
468 transformed *A. tumefaciens* strains were mixed equally (final OD_{600nm} = 0.3 per strain).
469 Subsequently, the bacterial resuspensions were infiltrated with a syringe into the abaxial site of
470 the *N. benthamiana* leaves.
471 Plants transformed with constructs under the control of an estradiol-inducible promotor system
472 (Zuo et al., 2000) were sprayed 2 – 4 days after infiltration and 6 – 16 h prior to sample
473 preparation for imaging or CoIP with an estradiol solution (10 µM ß-estradiol, 0.1 % v/v
474 Tween-20). Constitutive expressing transgenes (under the control of the *UBQ10* promotor)
475 were used for analyses 3 days after infiltration.

476 **Stable transformation of *A. thaliana***

477 To generate stable expression lines, parental *A. thaliana* plants were transformed 4 – 6 weeks
478 after germination via the floral dip method using *A. tumefaciens* GV3101 pMP90 pSoup
479 previously transformed with desired binary vectors (Suppl. Tab. 9, (Clough and Bent, 1998)).
480 Agrobacteria were cultivated overnight (28°C, shaking) in selective dYT medium (supplied
481 with 50 µg mL^{-1} rifampicin, 50 µg mL^{-1} gentamycin, 2.5 µg tetracycline, and 100 µg mL^{-1}
482 spectinomycin). 50 ml main cultures of the transgene-harboring Agrobacterium strains were
483 inoculated with 1 ml of an overnight preculture and centrifuged the next day (10 min, 4000 x
484 g, 4 °C). The pellet was resuspended in transformation medium (5 % w/v sucrose, 10 nM
485 $MgCl_2$, 0.01 % Silwet). Plants were prepared by removing already developed siliques and were
486 then subjected to floral dip. Whole shoots with special attention to the flowers were immersed
487 into the *A. tumefaciens* resuspension for 30 sec up to 5 min to guarantee the entry of bacteria
488 into the floral tissue, more precisely the female gametophyte. Afterwards, the plants were kept
489 under high humidity overnight at room temperature. Subsequently, the plants were cultivated
490 in standard phytochamber conditions until harvest. The t1 seeds were screened for positive
491 transformants by selection either for resistance against DL-phosphinothricin (PPT, alternatively
492 used in form of the herbicide BASTA®), or against hygromycin. Seeds of the transformed t0
493 plants were screened for positive transformants by selection either for resistance against DL-
494 phosphinothricin (PPT, alternatively used in form of the herbicide BASTA®), or against
495 hygromycin. T1 plants harboring transgenes with the BASTA® resistance cassette were selected
496 by spraying seedlings on soil (10 DAG) with a 120 mg/ml solution of BASTA®, or by sowing
497 the t1 seeds on ½ MS agar plates supplied with 10 µg/ml PPT. Transgenic plants with
498 hygromycin resistance were screened on ½ MS agar plates supplied with 15 µg/ml hygromycin.

499 Positive plants were further amplified for t2 selection and identification of homozygous lines.
500 All stable *A. thaliana* lines used and generated in this work are listed in Suppl. Tab. 10.

501 **Confocal microscopy and tissue staining**

502 *In vivo* fluorescence microscopy was performed at the CLSM systems Zeiss LSM 780 and Zeiss
503 LSM 880, respectively, employing C-Apochromat 40x/1.20 water objectives. For whole leaf
504 imaging and quantifying stomata (Fig. 7, Suppl. Fig. 16) a Plan-Apochromat 10x/0.45 M27 air
505 objective was used. Samples containing GFP derivates were excited with an argon laser at 488
506 nm and emission was detected at 490 – 530 nm by a 32-channel GaAsP detector or the Airyscan
507 detector system with a BP 495-550 / BP 570-620 filter set. The argon laser was also used for
508 excitation of mVenus at 514 nm, followed by measuring the emission at 520 – 550 nm with a
509 GaAsP detector. Diode-pumped solid state (DPSS) lasers were employed to excite mCh at
510 561 nm. Emission was detected by photomultiplier tubes (PMTs) in the range of 570 – 650 nm.
511 Propidium iodide (PI) was utilized to stain cell walls in roots (25 µM), shoot meristems (5 mM),
512 and leaf epidermis (50 µM). To quantify CSC layers, roots were subjected to mPS-PI staining
513 according to (Truernit et al., 2008), thereby marking cell walls and starch granules in
514 differentiated columella cells. PI was excited at 561 nm by DPSS lasers and detected by PMTs
515 at 590 – 650 nm. Alternatively, cell walls were counterstained with DAPI, which was excited
516 at 405 nm with a laser diode and emission was recorded at 410 – 480 nm by PMTs. To visualize
517 sieve plates of SEs, roots of Arabidopsis seedlings were incubated for 5 min in 0.01 % w/v
518 aniline blue, subsequently rinsed in a washing solution (10 mM KCl, 10 mM $CaCl_2$, 5 mM
519 NaCl), and imaged (excitation with a 405 nm diode, emission detected at 470 – 530 nm with
520 PMTs).

521 **FRET-FLIM interaction analysis**

522 FRET-FLIM experiments were conducted at a Zeiss LSM 780 (C-Apochromat 40x/1.20 water
523 objective) equipped with a single-photon counting device (PicoQuant Hydra Harp 400) and a
524 linear polarized diode laser (LDH-D-C-485). GFP or mNeonGreen donor fluorophores were
525 excited at 485 nm with a pulsed laser at a frequency of 32 MHz. Excitation power was adjusted
526 to 1 µW. Emission was detected in perpendicular and parallel polarization by Tau-SPADs
527 (PicoQuant) with a band-pass filter (520/35 AHF). Images were acquired with a frame size of
528 256 x 256, zoom 8, and a pixel dwell time of 12.6 µs. For each measurement 60 frames were
529 taken and the intensity-weighted mean lifetimes τ [ns] were calculated using PicoQuant
530 SymPhoTime64 software applying a biexponential fit. The displayed data were obtained from
531 at least 3 independent experiments.

532 **Protein extraction and CoIP**

533 Plant material was collected and immediately frozen in liquid N_2. All following steps were
534 performed at 4 °C. To identify novel CLV1 interactors via CoIP, whole Arabidopsis seedlings
535 were used (grown in liquid ½ MS, continuous light, gently shaking). Medium was removed 7
536 DAG and plants were grinded in liquid N_2 with mortar and pestle to obtain fine powder. Per
537 sample 500 mg material was mixed with 750 µl extraction buffer (EB: 50 mM Tris/HCl pH 7.5,
538 150 mM NaCl, 1 mM EDTA, 10 % v/v glycerol, 0.1 % v/v Nonident P40 substitute, 5 µM
539 dithiothreitol (DTT), 1 tablet of cOmplete™ proteinase inhibitor cocktail dissolved in 50 ml
540 EB). For interaction assays, 6 leaf discs (6 mm diameter, ~ 300 mg fresh weight) from
541 transiently transformed *N. benthamiana* leaves were grinded in a tube with two glass beads
542 (3 mm) with a TissueLyser II (Qiagen) and directly after supplied with 600 µl EB. Samples
543 dissolved in EB were incubated on a rotator for 1.5 h and subsequently centrifuged (20 min, 17
544 x g). The supernatant was collected for immunodetection via sodium dodecyl sulfate
545 polyacrylamide gel electrophoresis (SDS-PAGE, standard protocol of NEXT-GEL® with 10 %
546 acrylamide, samples were mixed with loading buffer (5 x: 200 mM Tris/HCl pH 6.8, 8 % w/v
547 SDS, 40 % v/v glycerol, 0.05 % w/v bromophenol blue, 50 mM DTT), and boiled 5 min at
548 95 °C prior to loading) and Western Blot (WB, wet electroblotting system, 80 min / 100 V)
549 analysis or used as input material for CoIP.
550 For CoIP experiments 500 µl protein extract was mixed with 25 µl calibrated anti-GFP
551 magnetic beads (ChromoTek GFP-Trap®) and incubated on a rotator for 2 h. After, supernatant
552 was discarded and beads were washed 4 times with washing buffer (10 mM Tris/HCl pH 7.5,
553 150 mM NaCl, 0.5 mM EDTA). Loaded beads were subjected to mass spectrometry or proteins
554 were eluted from beads by mixing with double concentrated loading buffer and boiling (95 °C
555 / 5 min) for analysis via SDS-PAGE, WB, and alkaline phosphatase (AP)-based
556 immunostaining. To detect GFP-fusion proteins, primary GFP antibodies (IgG, rat monoclonal,
557 diluted 1:1500 in blocking solution, incubation overnight at 4°C) and secondary anti-rat-AP
558 antibodies (1:5000, 2.5 h, room temperature) were applied. To detect RFP derivates, primary
559 RFP antibodies (IgG, mouse monoclonal, 1:1500, overnight, 4 °C) and secondary goat anti-
560 mouse IgG AP antibodies (1:5000, 2.5 h, room temperature) were used.

561 **Mass spectrometric analysis**

562 Mass spectrometry was performed at the Molecular Proteomics Laboratory (MPL, BMFZ,
563 HHU Düsseldorf). After immunoprecipitation of samples with anti-GFP beads (free GFP n=5,
564 CLV1-2xGFP n=5, CLV1-2xGFP + 5µM CLV3 peptide n=4), precipitated proteins were eluted

565 with 25 µl sample buffer (7.5% v/v glycerine, 3% w/v SDS and 37.5 mM 2-Amino-2-
566 (hydroxymethyl)-1,3-propanediol in water, pH 7) for 10 minutes at 90°C. Samples were further
567 processed by in-gel digestion with trypsin including reduction with dithiothreitol and alkylation
568 with iodoacetamide as described (Grube et al., 2018). Resulting peptides were resuspended in
569 0.1% trifluoroacetic acid and about half of the sample from each immunoprecipitation analyzed
570 by liquid chromatography coupled mass spectrometry as previously described (Ingold et al.,
571 2018). Briefly, peptides were separated on C18 material on an Ultimate 3000 rapid separation
572 liquid chromatography system (Thermo Fisher Scientific) using a one-hour gradient and
573 injected into a QExactive plus mass spectrometer (Thermo Fisher Scientific) via a nano
574 electrospray source interface. The mass spectrometer was operated in data dependent, positive
575 mode. First, survey scans were recorded (resolution 70000, scan range 200 – 2000 m/z) and
576 subsequently, up to twenty > 1 charged precursors ions were selected by the build-in
577 quadrupole, fragmented by higher-energy collisional dissociation and MS/MS spectra recorded
578 at a resolution of 17500.
579 Data analysis was carried out with MaxQuant (version 1.6.0.16, Max Planck Institute for
580 Biochemistry, Planegg, Germany) with standard parameters if not stated otherwise and using
581 the *A. thaliana* reference proteome sequences (UP000006548, downloaded on 2nd February
582 2017 from UniProt) supplemented with two entries for CLV1-2xGFP and free GFP. The "match
583 between runs" function and label-free quantification was enabled. Peptides and proteins were
584 accepted for identification with a false discovery rate of 1%. Only proteins identified with at
585 least two different peptides were considered as identified. Precursor intensity-based
586 quantification data was further analyzed using the Perseus framework (version 1.6.0.7, Max
587 Planck Institute for Biochemistry, Planegg, Germany).

588 **Reverse transcriptase quantitative real-time PCR (RT-qPCR)**

589 To evaluate the amount of residual *MAZ* transcripts in *maz-1* plants, RNA from seedlings 7
590 DAG was extracted with the Qiagen RNeasy Plant mini kit and 2 µg RNA per reaction was
591 used for first strand cDNA synthesis via SuperScript™ III reverse transcriptase (according
592 manufacture's protocol with oligo$(dT)_{18}$). The qPCR reactions were performed with
593 SsoAdvanced™ Universal SYBR® Green Supermix in a Stratagene Mx3005P qPCR System
594 (Agilent Technologies) with an optimized dilution of cDNA (accessed via dilution series for
595 each oligo pair). Applied oligonucleotides are listed in Suppl. Tab. 11. Data were normalized
596 to the housekeeping genes AT2G28390, AT4G34270, and At4g26410. Technical triplicates of
597 3 biological replicates were considered for each condition.

598 **Evaluation of mutant morphology**

599 Carpel number per silique of different *A. thaliana* mutants grown on soil under LD and
600 continuous light conditions, respectively, were quantified from 10 – 15 plants per genotype and
601 15 – 30 siliques per plant. Root length of seedlings 10 DAG was accessed after cultivation of
602 the examined genotypes on ½ MS plates supplied with synthetic CLV3 peptide in the indicated
603 concentrations. Measurements were done with ImageJ after scanning the plates. For each
604 condition at least 67 (and up to 113) single roots were measured and normalized to the mean of
605 the Col-0 samples of the same peptide concentration.
606 Root hair length and density of seedlings 5 DAG were quantified after cultivation on ½ MS and
607 image acquisition with a Nikon SMZ25 stereomicroscope. Per genotype 20 – 25 roots were
608 analyzed, in total with 3542 (Col-0), 975 (*fer-4*), 2433 (*mri-2*), and 4360 (*maz-1*) single
609 measurements. For each seedling, the length of all root hairs in focus on one side of the root
610 were determined.
611 Stomata cluster in cotyledons and leaves of seedlings 14 DAG grown on ½ MS were analyzed
612 after PI staining and imaging by counting total number of stomata and abundance of directly
613 adjacent stomata. For each genotype 5 – 10 cotyledons and 6 – 10 true leaves were examined
614 by counting all stomata in 4 distinct regions (400 x 400 µm) of each sample.

615 **Evaluation of mutant physiologic responses**

616 Drought stress experiments to access potential involvement of the *maz-1* allele in ABA
617 responses were performed with plants of different genetic background grown on soil under
618 standard conditions. Two weeks after germination seedlings were subjected to water deficiency
619 for either 10 days or 20 days and were subsequently re-watered to monitor recovery. Both, the
620 10 days and 20 days drought period approaches, included 3 pots of plants for each genotype,
621 which were randomly distributed on the tray.
622 Water-loss assays were conducted to estimate the degree of evaporation via open stomata after
623 dissection of 6 rosette leaves per sample (1 sample = 1 individual plant). For each genotype 8
624 samples (per repeat) were weighted at indicated time points. The reduction of weight was taken
625 as an approximation for water-loss. The assay was performed in three independent repeats.

626 **Software**

627 Statistical analyses and data plotting were realized with GraphPad Prism v 8. For visualization
628 and quantification of microscopic data ZEN (Zeiss, Black Version) and ImageJ v 1.51
629 (Schneider et al., 2012) was employed. The following prediction tools were used: CSS-Palm

630 4.0 (Ren et al., 2008), PredGPI (Pierleoni et al., 2008), Myristoylator by ExPASy (Bologna et
631 al., 2004), UbPred (Radivojac et al., 2010), UbiSite (Huang et al., 2016), BDM-PUB v 1.0.
632 Cloning was organized via Vector NTI® software. Protein alignments were done with ClustalΩ
633 (Sievers et al., 2011), phylogenetic analyses with MEGA X (Kumar et al., 2018), and tree
634 visualization with iTOL v 4 (Letunic and Bork, 2019).

635

636 **Acknowledgements**

637 P.B. was supported by the IMPRS *Understanding complex plant traits using computational and*
638 *evolutionary approaches*, work in R.S. lab is supported by the DFG through CRC1208 and
639 CEPLAS (EXC 2048). We thank Cornelia Gieseler, Silke Winters, and Carin Theres for
640 technical support, Aurélien Boisson-Dernier and Zachary Nimchuk for sharing Arabidopsis
641 seeds, Grégoire Denay, Rebecca Burkart, Marc Somssich, Frederic Boyer, and Pauline Anne
642 for sharing plasmids, Dolf Weijers and Mark Roosjen for the "sticky list" of typical GFP control
643 pull-downs, Vicky Howe for critical reading of the manuscript, the Center for Advanced
644 imaging (CAi) at HHU for microscopy support, and Gereon Poschmann from the Molecular
645 Proteomics Laboratory (MPL) at HHU for mass spec analyses.

646

647 **Authors contributions**

648 R.S. and P.B. conceived and planed the project. P.B. conducted experiments and data analyses,
649 besides the following: J.S. performed shoot meristem imaging and image processing, S.B. did
650 FLIM interaction studies of CLV1-mNeonG vs. Pti1-like homologs (Fig. 3 C), K.P. acquired
651 initial stomatal cluster rate data (Suppl. Fig. 15). P.B. and R.S. wrote the manuscript.

652 **Main figures**

653 **Figure 1** Expression patterns of *CLV1:CLV1-2xGFP* in different tissues of Arabidopsis.

654 **Figure 2** *In vivo* interaction analysis of MAZ and CLV1 via CoIP and FLIM.

655 **Figure 3** FLIM interactome of CLVf receptors and related signaling elements with the Pti1-like
656 family.

657 **Figure 4** Subcellular localization of MAZ at the PM depends on conserved palmitoylation sites.

658 **Figure 5** Expression analysis of *MAZ:MAZ-eGFP*//Col-0.

659 **Figure 6** *Maz-1* mutants show no increased carpel number but are partially resistant against
660 CLE peptide treatment.

661 **Figure 7** *Clv1-20;maz-1* double mutants display significantly increased stomata cluster rates.

662 **Figure 8** Model of MAZ as a signaling hub downstream of CLVf receptors.

663

664 **Supplementary material**

665 **Supplemental Figure 1** Expression domains of *CLV1* and *MAZ* in the vasculature of
666 Arabidopsis roots.

667 **Supplemental Figure 2** Two independent CoIP repetitions of CLV1-GFP with MAZ-mCherry.

668 **Supplemental Figure 3** Subcellular localization of MAZ in *N. benthamiana* leaf epidermis
669 cells.

670 **Supplemental Figure 4** Predicted palmitoylation sites at the N-terminus of MAZ are
671 mandatory for PM-localization.

672 **Supplemental Figure 5** Expression pattern of the transcriptional reporter *MAZ:mVenus-*
673 *NLS*//Col-0 in the root (3 DAG).

674 **Supplemental Figure 6** MAZ expression by MAZ promotor in different translational
675 reporters.

676 **Supplemental Figure 7** Expression of *MAZ:MAZ-eGFP* in the SAM of 5 weeks old
677 *A. thaliana*.

678 **Supplemental Figure 8** Co-localization of CLV1-eGFP and MAZ-mCherry in shoot and root.

679 **Supplemental Figure 9** Characterization of the *maz-1* allele GABI-Kat 485F03.

680 **Supplemental Figure 10** Carpel number of m*az-1* mutants is wild typic in continuous light
681 (CL).

682 **Supplemental Figure 11** *Maz-1* mutants are partially resistant to CLE40 peptide treatment in
683 terms of columella stem cell (CSC) layer specification.

684 **Supplemental Figure 12** The *maz-1* mutant does not display defects in root hair development.

685 **Supplemental Figure 13** Water loss assay of Arabidopsis leaves to monitor potential
686 differential stomata closure as an indication for a role of Pti1-homologs in ABA signaling.

687 **Supplemental Figure 14** Drought stress assay revealed no clear differences between the
688 analyzed genotypes to cope with water deficiency.

689 **Supplemental Figure 15** Impact of the *clv1-20* allele and CLE40 peptide treatment on stomata
690 development and clustering in Arabidopsis seedlings.

691 **Supplemental Figure 16** Cotyledons of *clv1-20*, *maz-1*, and the double mutant *clv1-20;maz-1*
692 display no significant changes of stomata density and cluster rate.

693

694 **Supplemental Table 1** Via mass spectroscopy identified proteins in CoIP fraction against
695 CLV1-2xGFP, which are not found in GFP-only control samples.

696 **Supplemental Table 2** Mean FRET efficiencies of tested donor-acceptor combinations at the
697 PM of transiently transformed *N. benthamiana* epidermis cells.

698 **Supplemental Table 3** Pti1-like family in *Arabidopsis thaliana* and predicted PM-localization
699 mechanisms.

700 **Supplemental Table 4** Chemicals.

701 **Supplemental Table 5** Analyzed *A. thaliana* mutants (Col-0 background).

702 **Supplemental Table 6** Genotyping strategies to verify listed mutant alleles.

703 **Supplemental Table 7** Entry plasmids.

704 **Supplemental Table 8** Plasmids used for transient gene expression in *N. benthamiana*.

705 **Supplemental Table 9** Plasmids used for stabile transformation of *A. thaliana*.

706 **Supplemental Table 9** Transgenic *A. thaliana* lines applied and generated in this study.

707 **Supplemental Table 11** Oligonucleotides for RT-qPCR.

708

709 **Appendix** Sequence alignment with ClustalΩ of Arabidopsis Pti1-like family and SlPti1.

References

Anne, P., Amiguet-Vercher, A., Brandt, B., Kalmbach, L., Geldner, N., Hothorn, M., and Hardtke, C.S. (2018). CLERK is a novel receptor kinase required for sensing of root-active CLE peptides in Arabidopsis. Development **145**: dev162354.

Anne, P. and Hardtke, C.S. (2018). Phloem function and development — biophysics meets genetics. Current Opinion in Plant Biology **43**: 22–28.

Anthony, R.G., Khan, S., Costa, J., Pais, M.S., and Bögre, L. (2006). The Arabidopsis protein kinase PTI1-2 is activated by convergent phosphatidic acid and oxidative stress signaling pathways downstream of PDK1 and OXI1. Journal of Biological Chemistry **281**: 37536–37546.

Bergmann, D.C. and Sack, F.D. (2007). Stomatal Development. Annual Review of Plant Biology **58**: 163–181.

Betsuyaku, S., Takahashi, F., Kinoshita, A., Miwa, H., Shinozaki, K., Fukuda, H., and Sawa, S. (2011). Mitogen-activated protein kinase regulated by the CLAVATA receptors contributes to shoot apical meristem homeostasis. Plant and Cell Physiology **52**: 14–29.

Bi, G., Zhou, Z., Wang, W., Li, L., Rao, S., Wu, Y., Zhang, X., Menke, F.L.H., Chen, S., and Zhou, J.M. (2018). Receptor-like cytoplasmic kinases directly link diverse pattern recognition receptors to the activation of mitogen-activated protein kinase cascades in Arabidopsis. Plant Cell **30**: 1543–1561.

Bleckmann, A., Weidtkamp-Peters, S., Seidel, C.A.M., and Simon, R. (2010). Stem cell signaling in Arabidopsis requires CRN to localize CLV2 to the plasma membrane. Plant Physiology **152**: 166–176.

Boisson-Dernier, A., Franck, C.M., Lituiev, D.S., and Grossniklaus, U. (2015). Receptor-like cytoplasmic kinase MARIS functions downstream of CrRLK1L-dependent signaling during tip growth. PNAS **112**: 12211–12216.

Bologna, G., Yvon, C., Duvaud, S., and Veuthey, A.-L. (2004). N-Terminal myristoylation predictions by ensembles of neural networks. Proteomics **4**: 1626–1632.

Bommert, P., Je, B. il, Goldshmidt, A., and Jackson, D. (2013). The maize Gα gene COMPACT PLANT2 functions in CLAVATA signalling to control shoot meristem size. Nature **502**: 555–558.

Brand, U., Fletcher, J.C., Hobe, M., Meyerowitz, E.M., and Simon, R. (2000). Dependence of stem cell fate in Arabidopsis on a feedback loop regulated by CLV3 activity. Science **289**: 617–9.

Breda, A.S., Hazak, O., Schultz, P., Anne, P., Graeff, M., Simon, R., and Hardtke, C.S. (2019). A Cellular Insulator against CLE45 Peptide Signaling. Current Biology **29**: 2051–2508.

Chen, S., Liu, J., Liu, Y., Chen, L., Sun, T., Yao, N., Wang, H.-B., and Liu, B. (2019). BIK1 and ERECTA Play Opposing Roles in Both Leaf and Inflorescence Development in Arabidopsis. Frontiers in Plant Science **10**: 1480.

Clough, S.J. and Bent, A.F. (1998). Floral dip: A simplified method for Agrobacterium-mediated transformation of Arabidopsis thaliana. Plant Journal **16**: 735–743.

Cui, Y., Hu, C., Zhu, Y., Cheng, K., Li, X., Wei, Z., Xue L., Lin, F., Shi, H., Yi, J., Hou, S, He, K., Li, J., and Gou, X. (2018). CIK receptor kinases determine cell fate specification during early anther development in Arabidopsis. Plant Cell **30**: 2383–2401.

Depuydt, S., Rodriguez-Villalon, A., Santuari, L., Wyser-Rmili, C., Ragni, L., and Hardtke, C.S. (2013). Suppression of Arabidopsis protophloem differentiation and root meristem growth by CLE45 requires the receptor-like kinase BAM3. PNAS **110**: 7074–9.

DeYoung, B.J., Bickle, K.L., Schrage, K.J., Muskett, P., Patel, K., and Clark, S.E. (2006). The CLAVATA1-related BAM1, BAM2 and BAM3 receptor kinase-like proteins are required for meristem function in Arabidopsis. Plant Journal **45**: 1–16.

Deyoung, B.J. and Clark, S.E. (2008). BAM receptors regulate stem cell specification and organ development through complex interactions with CLAVATA signaling. Genetics **180**: 895–904.

Fan, M., Ma, W., Liu, C., Zhang, C., Wu, S., Chen, M., Liu, K., Cai, F., and Lin, F. (2018). Evolution and expression characteristics of receptor-like cytoplasmic protein kinases in maize, rice and Arabidopsis. International Journal of Molecular Sciences **19**(11): 3680.

Fiers, M., Golemiec, E., Xu, J., van der Geest, L., Heidstra, R., Stiekema, W., and Liu, C.M. (2005). The 14-amino acid CLV3, CLE19, and CLE40 peptides trigger consumption of the root meristem in Arabidopsis through a CLAVATA2-dependent pathway. Plant Cell **17**: 2542–2553.

Fletcher, J.C., Brand, U., Running, M.P., Simon, R., and Meyerowitz, E.M. (1999). Signaling of cell fate decisions by CLAVATA3 in Arabidopsis shoot meristems. Science **283**: 1911–4.

Forzani, C., Carreri, A., de La Fuente Van Bentem, S., Lecourieux, D., Lecourieux, F., and Hirt, H. (2011). The Arabidopsis protein kinase Pto-interacting 1-4 is a common target of the oxidative signal-inducible 1 and mitogen-activated protein kinases. FEBS Journal **278**: 1126–1136.

Fukuda, H. and Hardtke, C.S. (2020). Peptide signaling pathways in vascular differentiation. Plant Physiology **182**: 1636–1644.

Gagne, J.M. and Clark, S.E. (2010). The Arabidopsis stem cell factor POLTERGEIST is membrane localized and phospholipid stimulated. Plant Cell **22**: 729–43.

Geisler, M., Nadeau, J., and Sack, F.D. (2000). Oriented asymmetric divisions that generate the stomatal spacing pattern in Arabidopsis are disrupted by the too many mouths mutation. Plant Cell **12**: 2075–2086.

Grube, L., Dellen, R., Kruse, F., Schwender, H., Stühler, K., and Poschmann, G. (2018). Mining the Secretome of C2C12 Muscle Cells: Data Dependent Experimental Approach to Analyze Protein Secretion Using Label-Free Quantification and Peptide Based Analysis. Journal of Proteome Research **17**: 879–890.

Guo, X., Wang, J., Gardner, M., Fukuda, H., Kondo, Y., Etchells, J.P., Wang, X., and Mitchum, M.G. (2017). Identification of cyst nematode B-type CLE peptides and modulation of the vascular stem cell pathway for feeding cell formation. PLOS Pathogens **13**: e1006142.

Hanemian, M.,Barlet, X., Sorin, C., Yadeta, K., Keller, H., Favery, B., Simon, R., Thomma, B., Hartmann, C., Crespi, M., Marco, Y., Tremousaygue, D., and Deslandes, L. (2016). Arabidopsis CLAVATA 1 and CLAVATA2 receptors contribute to Ralstonia solanacearum pathogenicity through a miR169-dependent pathway. New Phytologist **211**: 502–515.

Hara, K., Kajita, R., Torii, K.U., Bergmann, D.C., and Kakimoto, T. (2007). The secretory peptide gene EPF1 enforces the stomatal one-cell-spacing rule. Genes and Development **21**: 1720–1725.

Hazak, O., Brandt, B., Cattaneo, P., Santiago, J., Rodriguez-Villalon, A., Hothorn, M., and Hardtke, C.S. (2017). Perception of root-active CLE peptides requires CORYNE function in the phloem vasculature. EMBO reports **18**: 1367–1381.

He, Y., Zhou, J., Shan, L., and Meng, X. (2018). Plant cell surface receptor-mediated signaling - A common theme amid diversity. Journal of Cell Science **131**: jcs209353.

Heazlewood, J.L., Durek, P., Hummel, J., Selbig, J., Weckwerth, W., Walther, D., and Schulze, W.X. (2008). PhosPhAt: a database of phosphorylation sites in Arabidopsis thaliana and a plant-specific phosphorylation site predictor. Nucleic Acids Research **36**: 1015–1021.

Hellens, R.P., Anne Edwards, E., Leyland, N.R., Bean, S., and Mullineaux, P.M. (2000). pGreen: A versatile and flexible binary Ti vector for Agrobacterium-mediated plant transformation. Plant Molecular Biology **42**: 819–832.

Herrmann, M.M., Pinto, S., Kluth, J., Wienand, U., and Lorbiecke, R. (2006). The PTI1-like kinase ZmPti1a from maize (Zea mays L.) co-localizes with callose at the plasma membrane of pollen and facilitates a competitive advantage to the male gametophyte. BMC Plant Biology **6**: 22.

Hu, C., Zhu, Y., Cui, Y., Cheng, K., Liang, W., Wei, Z., Zhu, M., Yin, H., Zeng, L., Xiao, Y., Lv, M., Yi, J., Hou, S., He, K., Li, J., and Gou, X. (2018). A group of receptor kinases are essential for CLAVATA signalling to maintain stem cell homeostasis. Nature Plants **4**: 205–211.

Huang, C.H., Su, M.G., Kao, H.J., Jhong, J.H., Weng, S.L., and Lee, T.Y. (2016). UbiSite: Incorporating two-layered machine learning method with substrate motifs to predict ubiquitin-conjugation site on lysines. BMC Systems Biology **10**: S6.

Hurst, C.H. and Hemsley, P.A. (2015). Current perspective on protein S-acylation in plants: More than just a fatty anchor? Journal of Experimental Botany **66**(6): 1599–1606.

Ingold, I., Berndt, C., Schmitt, S., Doll, S., Poschmann, G., Buday, K., Roveri, A., Peng, X., Porto Freitas, F., Seibt, T., Mehr, L., Aichler, M., Walch, A., Lamp, D., Jastroch, M., Miyamoto, S., Wurst, W., Ursini, F., Arnér, E.S.J., Fradejas-Villar, N., Schweizer, U., Zischka, H., Angeli, J.P.F., and Conrad, M. (2018). Selenium Utilization by GPX4 Is Required to Prevent Hydroperoxide-Induced Ferroptosis. Cell **172**: 409-422.e21.

Ishida, T., Tabata R., Yamada, M., Aida, M., Mitsumasu, K., Fujiwara, M., Yamaguchi, K., Shigenobu, S., Higuchi, M., Tsuji, H., Shimamoto, K., Hasebe, M., Fukuda, H., and Sawa, S. (2014). Heterotrimeric G proteins control stem cell proliferation through CLAVATA signaling in Arabidopsis. EMBO reports **15**: 1202–1209.

Jeong, S., Trotochaud, A.E., and Clark, S.E. (1999). The Arabidopsis CLAVATA2 gene encodes a receptor-like protein required for the stability of the CLAVATA1 receptor-like kinase. Plant Cell **11**: 1925–1933.

Katzen, F. (2007). Gateway® recombinational cloning: A biological operating system. Expert Opinion on Drug Discovery **2**: 571–589.

Kayes, J.M. and Clark, S.E. (1998). CLAVATA2, a regulator of meristem and organ development in Arabidopsis. Development **125**: 3843–3851.

Kinoshita, A., Betsuyaku, S., Osakabe, Y., Mizuno, S., Nagawa, S., Stahl, Y., Simon, R., Yamaguchi-Shinozaki, K., Fukuda, H., and Sawa, S. (2010). RPK2 is an essential receptor-like kinase that transmits the CLV3 signal in Arabidopsis. Development **137**: 3911–3920.

Kumar, S., Stecher, G., Li, M., Knyaz, C., and Tamura, K. (2018). MEGA X: Molecular Evolutionary Genetics Analysis across Computing Platforms. Molecular Biology and Evolution **35**: 1547–1549.

Lampropoulos, A., Sutikovic, Z., Wenzl, C., Maegele, I., Lohmann, J.U., and Forner, J. (2013). GreenGate - a novel, versatile, and efficient cloning system for plant transgenesis. PloS one **8**: e83043.

Lee, H., Jun, Y.S., Cha, O.K., and Sheen, J. (2019). Mitogen-activated protein kinases MPK3 and MPK6 are required for stem cell maintenance in the Arabidopsis shoot apical meristem. Plant Cell Reports **38**: 311–319.

Lee, J.S., Kuroha, T., Hnilova, M., Khatayevich, D., Kanaoka, M.M., Mcabee, J.M., Sarikaya, M., Tamerler, C., and Torii, K.U. (2012). Direct interaction of ligand-receptor pairs specifying stomatal patterning. Genes and Development **26**: 126–136.

Letunic, I. and Bork, P. (2019). Interactive Tree Of Life (iTOL) v4: recent updates and new developments. Nucleic Acids Research **47**: W256–W259.

Li, Y. and Qi, B. (2017). Progress toward understanding protein S-acylation: Prospective in plants. Frontiers in Plant Science **8**: 346.

Liang, X. and Zhou, J.-M. (2018). Receptor-Like Cytoplasmic Kinases: Central Players in Plant Receptor Kinase–Mediated Signaling. Annual Review of Plant Biology **69**: 267–299.

Lin, W., Lu, D., Gao, X., Jiang, S., Ma, X., Wang, Z., Mengiste, T., He, P., and Shan, L. (2013). Inverse modulation of plant immune and brassinosteroid signaling pathways by the receptor-like cytoplasmic kinase BIK1. PNAS **110**: 12114–12119.

Lu, D., Wu, S., Gao, X., Zhang, Y., Shan, L., and He, P. (2010). A receptor-like cytoplasmic kinase, BIK1, associates with a flagellin receptor complex to initiate plant innate immunity. PNAS **107**: 496–501.

Mandel, T., Moreau, F., Kutsher, Y., Fletcher, J.C., Carles, C.C., and Williams, L.E. (2014). The ERECTA receptor kinase regulates Arabidopsis shoot apical meristem size, phyllotaxy and floral meristem identity. Development **141**: 830–841.

Matsui, H., Matsui, H., Fujiwara, M., Hamada, S., Shimamoto, K., Nomura, Y., Nakagami, H., Takahashi, A., and Hirochika, H. (2014). Plasma membrane localization is essential for oryza sativa pto-interacting protein 1a-mediated negative regulation of immune signaling in rice. Plant Physiology **166**: 327–336.

Mayer, K.F.X., Schoof, H., Haecker, A., Lenhard, M., Jürgens, G., and Laux, T. (1998). Role of WUSCHEL in regulating stem cell fate in the Arabidopsis shoot meristem. Cell **95**: 805–815.

Müller, R., Bleckmann, A., and Simon, R. (2008). The receptor kinase CORYNE of Arabidopsis transmits the stem cell-limiting signal CLAVATA3 independently of CLAVATA1. Plant Cell **20**: 934–946.

Nimchuk, Z.L., Tarr, P.T., and Meyerowitz, E.M. (2011a). An evolutionarily conserved pseudokinase mediates stem cell production in plants. Plant Cell **23**: 851–854.

Nimchuk, Z.L., Tarr, P.T., Ohno, C., Qu, X., and Meyerowitz, E.M. (2011b). Plant stem cell signaling involves ligand-dependent trafficking of the CLAVATA1 receptor kinase. Current Biology **21**: 345–352.

Nimchuk, Z.L., Zhou, Y., Tarr, P.T., Peterson, B.A., and Meyerowitz, E.M. (2015). Plant stem cell maintenance by transcriptional cross-regulation of related receptor kinases. Development **142**: 1043–1049.

Pierleoni, A., Martelli, P., and Casadio, R. (2008). PredGPI: A GPI-anchor predictor. BMC Bioinformatics **9**: 392.

Qi, X., Han, S.K., Dang, J.H., Garrick, J.M., Ito, M., Hofstetter, A.K., and Torii, K.U. (2017). Autocrine regulation of stomatal differentiation potential by EPF1 and ERECTA-LIKE1 ligand-receptor signaling. eLife **6**: e24102.

Qian, P., Song, W., Yokoo, T., Minobe, A., Wang, G., Ishida, T., Sawa, S., Chai, J., and Kakimoto, T. (2018). The CLE9/10 secretory peptide regulates stomatal and vascular development through distinct receptors. Nature Plants **4**: 1071–1081.

Radivojac, P., Vacic, V., Haynes, C., Cocklin, R.R., Mohan, A., Heyen, J.W., Goebl, M.G., and Iakoucheva, L.M. (2010). Identification, analysis, and prediction of protein ubiquitination sites. Proteins: Structure, Function and Bioinformatics **78**: 365–380.

Ren, J., Wen, L., Gao, X., Jin, C., Xue, Y., and Yao, X. (2008). CSS-Palm 2.0: an updated software for palmitoylation sites prediction. Protein Engineering, Design and Selection **21**: 639–644.

Rosas-Diaz, T., Zhang, D., Fan, P., Wang, L., Ding, X., Jiang, Y., Jimenez-Gongora, T., Medina-Puche, L., Zhao, X., Feng, Z., Zhang, G., Liu, X., Bejarano, E.R., Tan, L., Zhang, H., Zhu, J.-K., Xing, W., Faulkner, C., Nagawa, S., and Lozano-Duran, R. (2018). A virus-targeted plant receptor-like kinase promotes cell-to-cell spread of RNAi. PNAS **115**: 1388–1393.

Schneider, C.A., Rasband, W.S., and Eliceiri, K.W. (2012). NIH Image to ImageJ: 25 years of image analysis. Nature Methods **9**: 671–675.

Schoof, H., Lenhard, M., Haecker, A., Mayer, K.F.X., Jürgens, G., and Laux, T. (2000). The stem cell population of Arabidopsis shoot meristems is maintained by a regulatory loop between the CLAVATA and WUSCHEL genes. Cell **100**: 635–644.

Sessa, G., D'Ascenzo, M., and Martin, G.B. (2000). The major site of the Pti1 kinase phosphorylated by the Pto kinase is located in the activation domain and is required for Pto-Pti1 physical interaction. European Journal of Biochemistry **267**: 171–178.

Shimizu, N., Ishida, T., Yamada, M., Shigenobu, S., Tabata, R., Kinoshita, A., Yamaguchi, K., Hasebe, M., Mitsumasu, K., and Sawa, S. (2015). BAM 1 and RECEPTOR-LIKE PROTEIN KINASE 2 constitute a signaling pathway and modulate CLE peptide-triggered growth inhibition in Arabidopsis root. New Phytologist **208**: 1104–1113.

Shinohara, H. and Matsubayashi, Y. (2015). Reevaluation of the CLV3-receptor interaction in the shoot apical meristem: dissection of the CLV3 signaling pathway from a direct ligand-binding point of view. Plant Journal **82**: 328–36.

Shiu, S.H. and Bleecker, A.B. (2003). Expansion of the receptor-like kinase/Pelle gene family and receptor-like proteins in Arabidopsis. Plant Physiology **132**: 530–543.

Shiu, S.H., Karlowski, W.M., Pan, R., Tzeng, Y.H., Mayer, K.F.X., and Li, W.H. (2004). Comparative analysis of the receptor-like kinase family in Arabidopsis and rice. Plant Cell **16**: 1220–1234.

Sievers, F., Wilm, A., Dineen, D., Gibson, T.J., Karplus, K., Li, W., Lopez, R., McWilliam, H., Remmert, M., Söding, J., Thompson, J.D., and Higgins, D.G. (2011). Fast, scalable generation of high-quality protein multiple sequence alignments using Clustal Omega. Molecular Systems Biology **7**: 539.

Stahl, Y., Grabowski, S., Bleckmann, A., Kühnemuth, R., Weidtkamp-Peters, S., Pinto, K.G., Kirschner, G.K., Schmid, J.B., Wink, R.H., Hülsewede, A., Felekyan, S., Seidel, C.A.M., Simon, R. (2013). Moderation of Arabidopsis root stemness by CLAVATA1 and ARABIDOPSIS CRINKLY4 receptor kinase complexes. Current Biology **23**: 362–71.

Stahl, Y. and Simon, R. (2012). Receptor Kinases in Plant Meristem Development. In Signaling and Communication in Plants, F. Tax and B. Kemmerling, eds (Springer: Berlin, Heidelberg), pp. 23–39.

Stahl, Y., Wink, R.H., Ingram, G.C., and Simon, R. (2009). A Signaling Module Controlling the Stem Cell Niche in Arabidopsis Root Meristems. Current Biology **19**(11): 909–914.

Tameshige, T., Ikematsu, S., Torii, K.U., and Uchida, N. (2017). Stem development through vascular tissues: EPFL-ERECTA family signaling that bounces in and out of phloem. J Exp Bot **68**: 45–53.

Truernit, E., Lè Ne Bauby, H., Dubreucq, B., Grandjean, O., Runions, J., Barthé Lé, J., and Palauqui, J.-C. (2008) High-Resolution Whole-Mount Imaging of Three-Dimensional Tissue Organization and Gene Expression Enables the Study of Phloem Development and Structure in Arabidopsis. Plant Cell **20**: 1494–1503.

Uchida, N., Shimada, M., and Tasaka, M. (2013). ERECTA-Family Receptor Kinases Regulate Stem Cell Homeostasis via Buffering its Cytokinin Responsiveness in the Shoot Apical Meristem. Plant and Cell Physiology **54**: 343–351.

Voinnet, O., Rivas, S., Mestre, P., and Baulcombe, D. (2003). An enhanced transient expression system in plants based on suppression of gene silencing by the p19 protein of tomato bushy stunt virus. Plant Journal **33**(5): 949–956.

Wang, J., Zhang, Q., Yu, Q., Peng, L., Wang, J., Dai, Q., Yang, Y., and Li, X. (2019). CARK6 is involved in abscisic acid to regulate stress responses in Arabidopsis thaliana. Biochemical and Biophysical Research Communications **513**(2): 460–464.

Wu, Q., Xu, F., Liu, L., Char, S.N., Ding, Y., Je, B. il, Schmelz, E., Yang, B., and Jackson, D. (2020). The maize heterotrimeric G protein β subunit controls shoot meristem development and immune responses. PNAS **117**: 1799–1805.

Xi, L., Wu, X.N., Gilbert, M., and Schulze, W.X. (2019). Classification and interactions of LRR receptors and co-receptors within the arabidopsis plasma membrane – An overview. Frontiers in Plant Science **10**: 472.

Zhang, L., DeGennaro, D., Lin, G., Chai, J., and Shpak, E.D. (2020). ERECTA family signaling constrains CLAVATA3 and WUSCHEL to the center of the shoot apical meristem. bioRxiv Developmental Biology: 2020.02.24.962787.

Zhang, L., Li, X., Li, D., Sun, Y., Li, Y., Luo, Q., Liu, Z., Wang, J., Li, X., Zhang, H., Lou, Z., and Yang, Y. (2018). CARK1 mediates ABA signaling by phosphorylation of ABA receptors. Cell Discovery **4**: 1–10.

Zhou, J., Loh, Y.T., Bressan, R.A., and Martin, G.B. (1995). The tomato gene Pti1 encodes a serine/threonine kinase that is phosphorylated by Pto and is involved in the hypersensitive response. Cell **83**: 925–935.

Zoulias, N., Harrison, E.L., Casson, S.A., and Gray, J.E. (2018). Molecular control of stomatal development. Biochemical Journal **475**: 441–454.

Zuo, J., Niu, Q.W., and Chua, N.H. (2000). An estrogen receptor-based transactivator XVE mediates highly inducible gene expression in transgenic plants. Plant Journal **24**: 265–273.

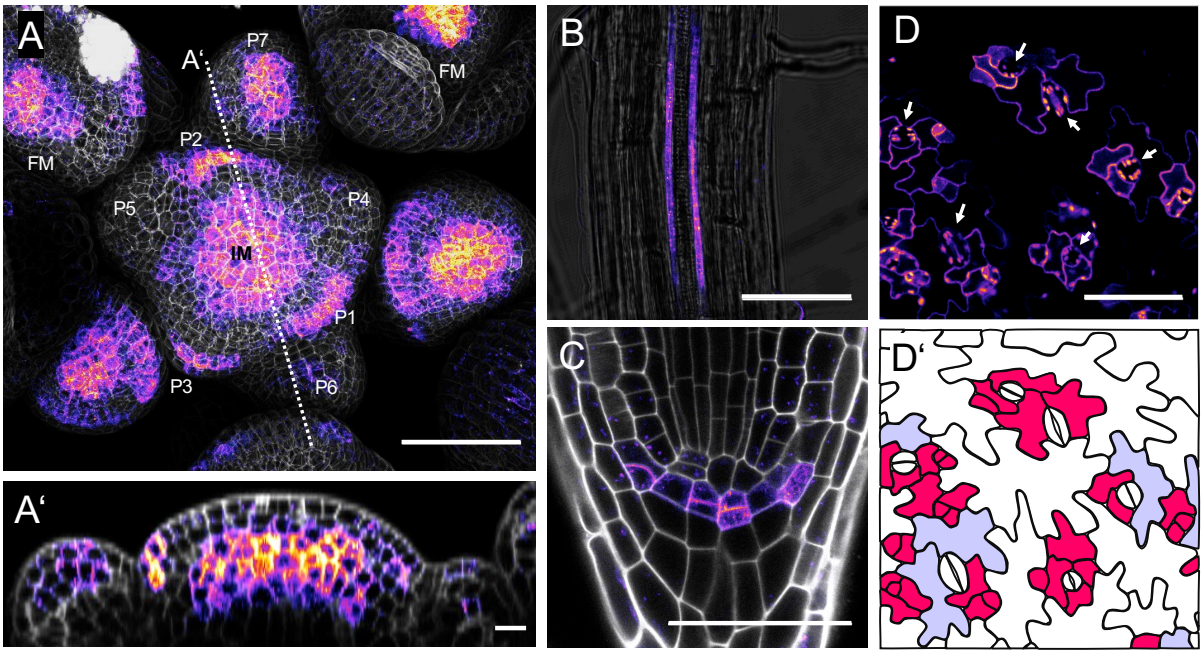

Figure 1 Expression patterns of *CLV1:CLV1-2xGFP* in different tissues of Arabidopsis.

A, A’ Inflorescence with inflorescence meristem (IM), floral primordia, and floral meristems (FM) of 5 weeks old *CLV1*:*CLV1-2xGFP//clv1-11* plants depicted as maximum intensity projection of a z-stack (A) and XZ section (A’) at indicated position. *CLV1* is expressed in the central zone of the meristems and in border cells toward newly arising primordia. **B** Root section within the differentiation zone of a seedling 5 DAG shows presence of the fusion protein CLV1-2xGFP in companion cell files (compare Suppl. Fig. 1 A). **C** Within the root meristem *CLV1* expression is restricted to columella stem cells and epidermis/lateral root cap initials (seedling 5 DAG). **D** In the epidermis of first true leaves (14 DAG) *CLV1-2xGFP* expression is predominantly found in cells of the stomata lineage. Guard cells (white arrows in D) show no expression at the PM (note autofluorescence of chloroplasts). **D’** The schematic representation of D illustrates outlines of all cells (based on bright field channel). Cells with clear GFP fluorescence signals at the PM are colored in pink, with weak signals in light blue. A, A’, C: merge of GFP channel (LUT: fire) and PI (grey). B: merge of GFP (fire) with bright field (grey). Scale bares: 50 µm (A, B, C, D) and 10 µm (A’).

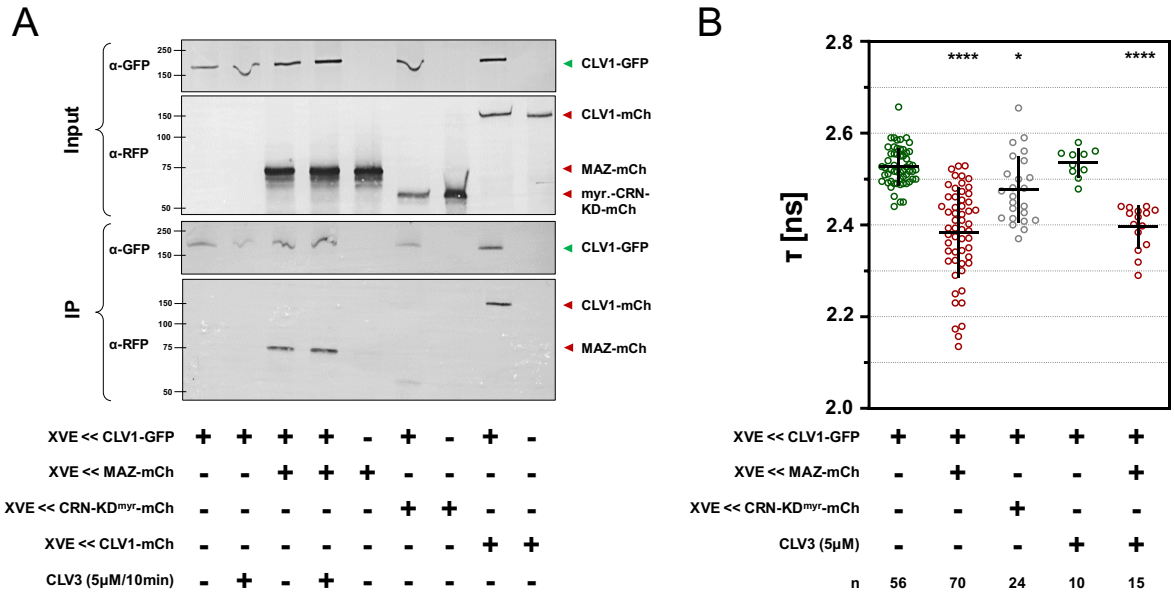

Figure 2 *In vivo* interaction analysis of MAZ and CLV1 via CoIP and FLIM.

CoIP and FLIM was performed with *N. benthamiana* leaf epidermis material transiently expressing combinations of indicated fluorophore fusions under the control of the *XVE<<oLexA-35S* estradiol inducible system. **A** MAZ-mCherry (mCh) is co-immunoprecipitated with CLV1-GFP using anti-GFP magnetic beads and subsequent immunodetection with antibodies against GFP and RFP, respectively. The negative control, myristoylated CRN-KD-mCh, is not pulled down together with CLV1-GFP, while the detection of CLV1-mCh reflects the previously reported homomerization of CLV1 (Bleckmann et al., 2010). Treatment of CLV3 peptide (5µM, 10 min prior to sample preparation) does not affect the interaction in this setup. **B** The fluorescence lifetime τ [ns] of CLV1-GFP is reduced in the presence of MAZ-mCh, while the PM control (CRN-KD^{myr}-mCh) reduces the τ of CLV1-GFP with low efficiency. Infiltration of a 5 µM CLV3 peptide solution into the leaves 5 – 15 min prior to measurements does not alter the τ values of donor-only nor FRET samples. Number of repetitions are indicated, p-values were calculated by ANOVA and Dunnett´s post hoc test, with * for $p \leq 0.05$, and **** for $p \leq 0.0001$. Error bars display SD.

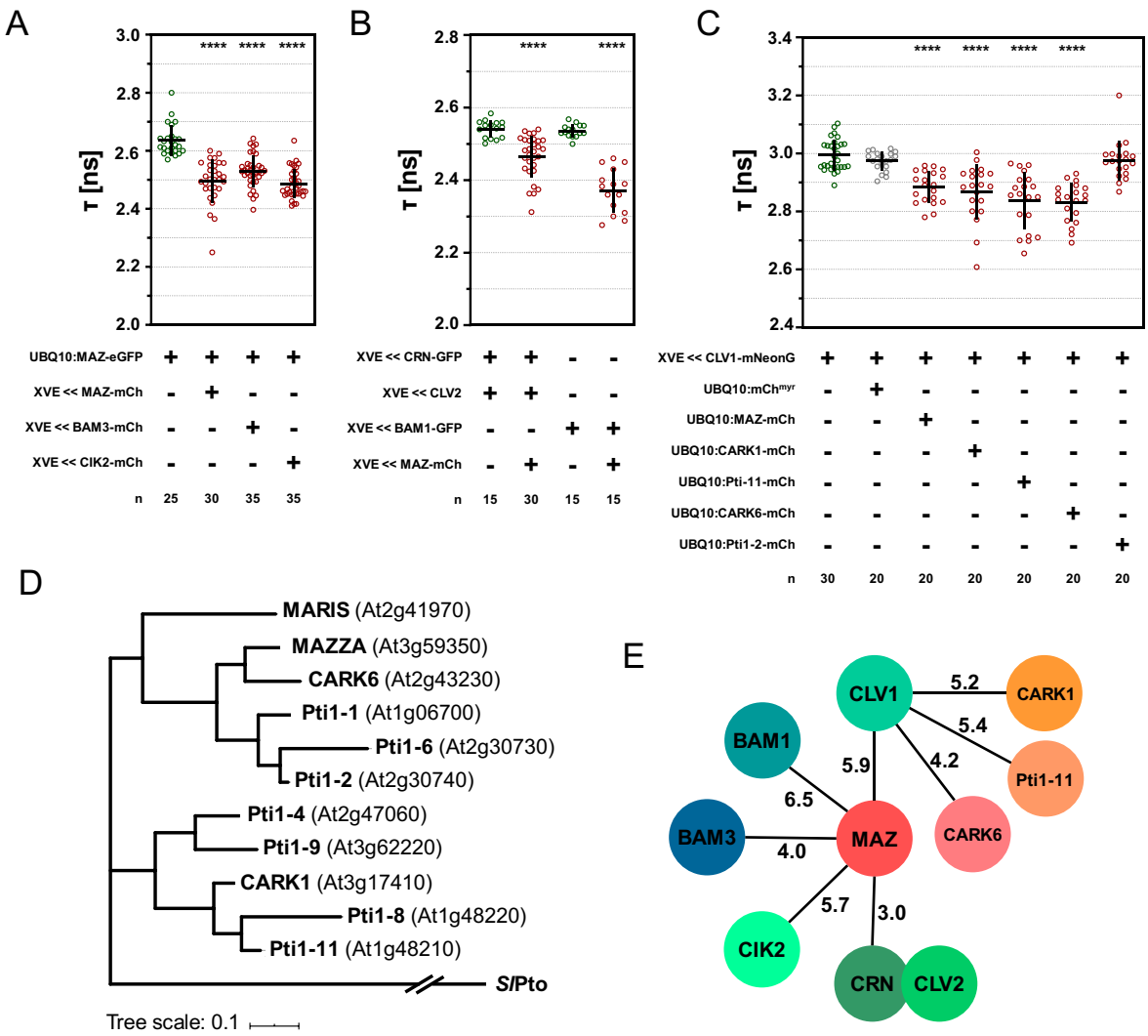

Figure 3 FLIM interactome of CLVf receptors and related signaling elements with the Pti1-like family.

A – C Fluorescence lifetime τ [ns] was determined in the *N. benthamiana* system, expressing the indicated constructs via the constitutive *UBQ10* promoter or under the control of the *XVE<<oLexA-35S* estradiol inducible module. **A** Donor τ of MAZ-eGFP is reduced in the presence of MAZ-mCh, BAM3-mCh, and CIK2-mCh, respectively. Note that the enhanced GFP variant (eGFP) was used here, explaining the slight differences compared to donor-only τ values in Fig 2 B and 3 B with constructs harboring the regular (F64) GFP. **B** The τ of CRN-GFP is decreased significantly but with a comparable low mean FRET efficiency of 3 % in the presence of MAZ-mCh and CLV2, while τ of BAM1-GFP is reduced with a FRET efficiency of 6.5 % by MAZ-mCh. **C** The τ of CLV1-mNeonGreen is significantly reduced in the presence of MAZ-mCh, CARK1-mCh, Pti1-11-mCh, CARK6-mCh, but not in combination with Pti1-2-mCh (nor by the negative control myristoylated mCh). Number of repetitions for FLIM experiments are indicated, p-values were calculated by ANOVA and Dunnett´s post hoc test, with **** for $p \leq 0.0001$. Error bars display SD. **D** Phylogram of the Pti1-homologs of *A. thaliana* and the *Solanum lycopersicum* SlPto as outgroup. The tree was generated after initial multiple sequence alignment (ClustalΩ) and subsequently applying a Maximum Likelihood strategy in MEGAX (via the JTT-matrix based model and 1000 repetitions). Final tree visualization was realized with iTOL software. Branch length is in scale as indicated displaying the calculated substitutions/site rate. **E** Graphical summary of the FLIM interactions identified here, mean FRET efficiency values are indicated for each pair (compare Suppl. Tab. 2).

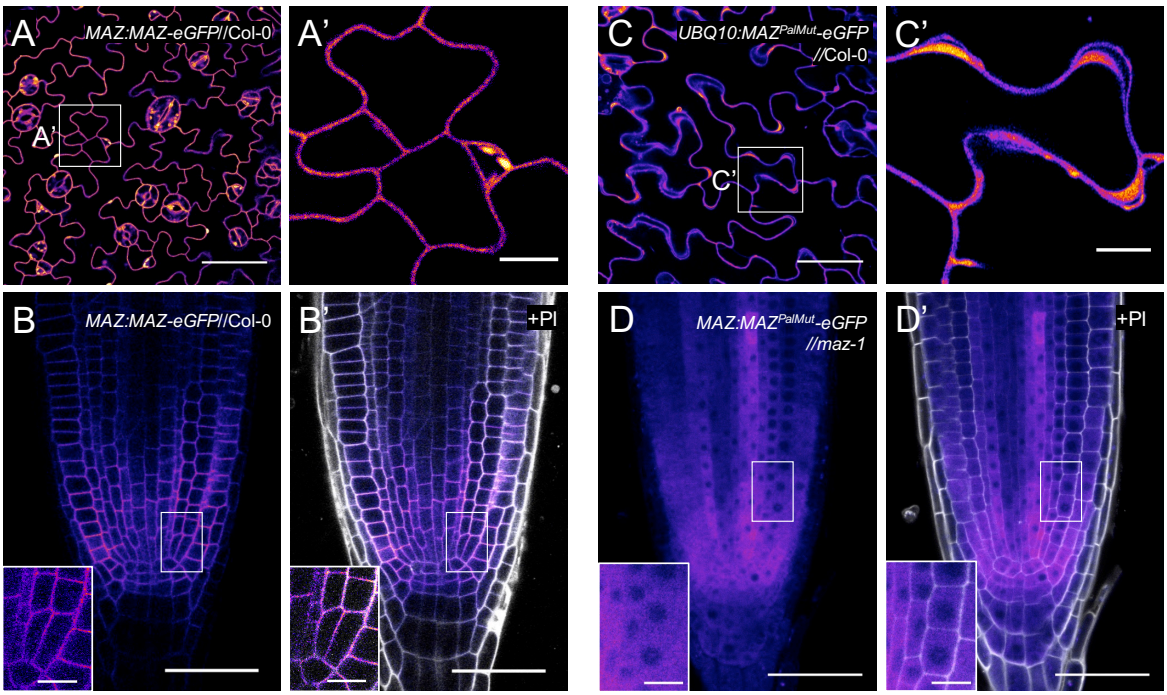

Figure 4 Subcellular localization of MAZ at the PM depends on conserved palmitoylation sites.

Stable expression of different MAZ variants demonstrate the impact of the predicted palmitoylation sites C48, C49 (and the adjacent C51) on subcellular localization of MAZ-eGFP. **A – B'** The wild typic MAZ protein (fused to eGFP) is located at the PM after expression under the native *MAZ* promotor, as shown here in rosette leaves (A, A') and in the root meristem (RM, B, B'). **C – D'** Site directed mutagenesis of the palmitoylation sites causes a shift of localization of the mutant MAZ^{PalMut}-eGFP fusion protein from the PM to the cytoplasm, both, when expressed under the *UBQ10* promotor, e.g. in leaf epidermis cells (C, C''), or under the control of the native *MAZ* promotor, shown here in the RM region. Sale bars: 50 µm (A, B, B', C, D, D'), 10 µm (A', C', detail views of B, B', D, D'). All images are displayed in the LUT fire, in B' and D' the merge with PI (grey) is shown.

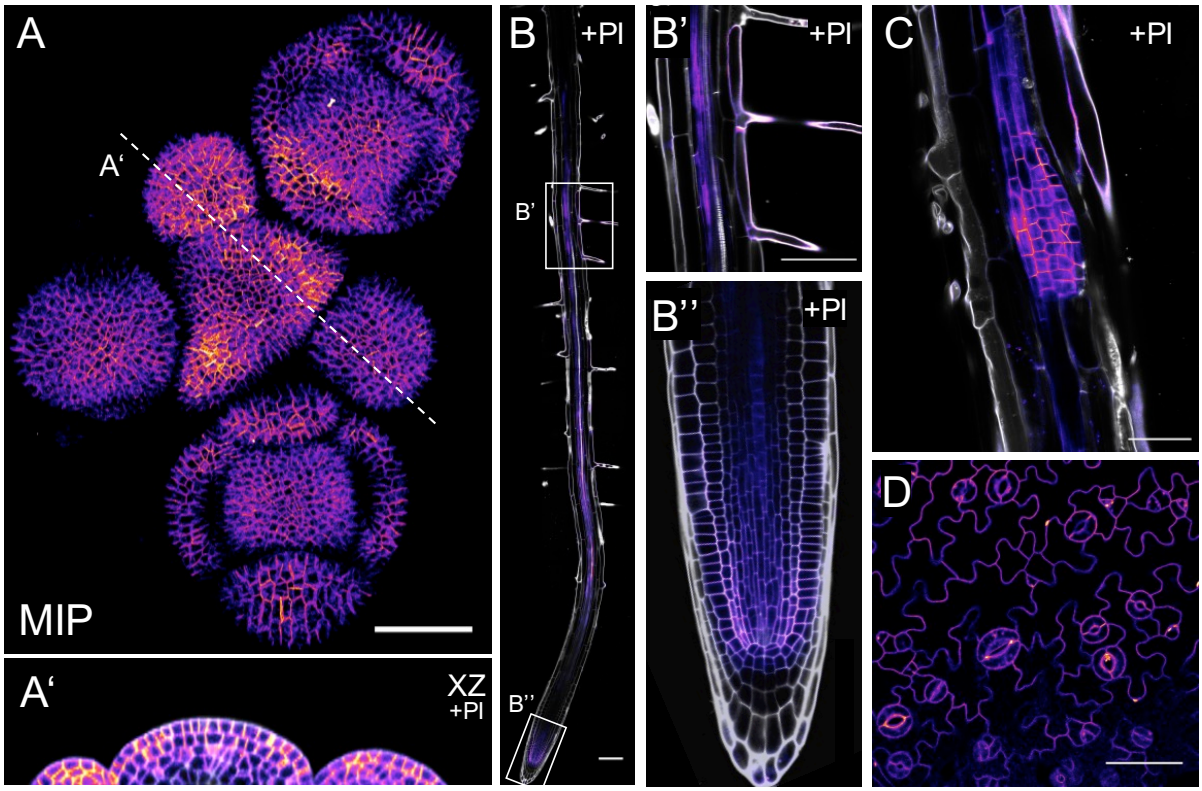

Figure 5 Expression analysis of *MAZ:MAZ-eGFP*//Col-0.

A, A’ Within the inflorescence, MAZ-eGFP is found in all cell layers. Z-stack acquired from a sample of a 5 weeks old plant, presented here as maximum intensity projection **(**MIP, A) and XZ section at indicated position (A’). *MAZ* expression is elevated at boundary regions towards newly formed primordia and towards organs in later stages of development. **B, B’, B’’** *MAZ* expression in the root (imaged 5 DAG) comprises the vasculature, root hairs (B’), and the root meristem (B’’). **C** Emerging lateral roots show distinct fluorescence signals of the MAZ-eGFP fusion (10 DAG, compare Suppl. Fig. 6). **D** In the epidermis of cotyledons (14 DAG), MAZ-eGFP is present in pavement cells, in the stomata lineage, and in mature guard cells. Scale bars: 50 µm (A, B’ – D), 10 µm (A’), 100 µm (B). GFP-signals visualized by the LUT fire, in A’ – C merge with PI (grey).

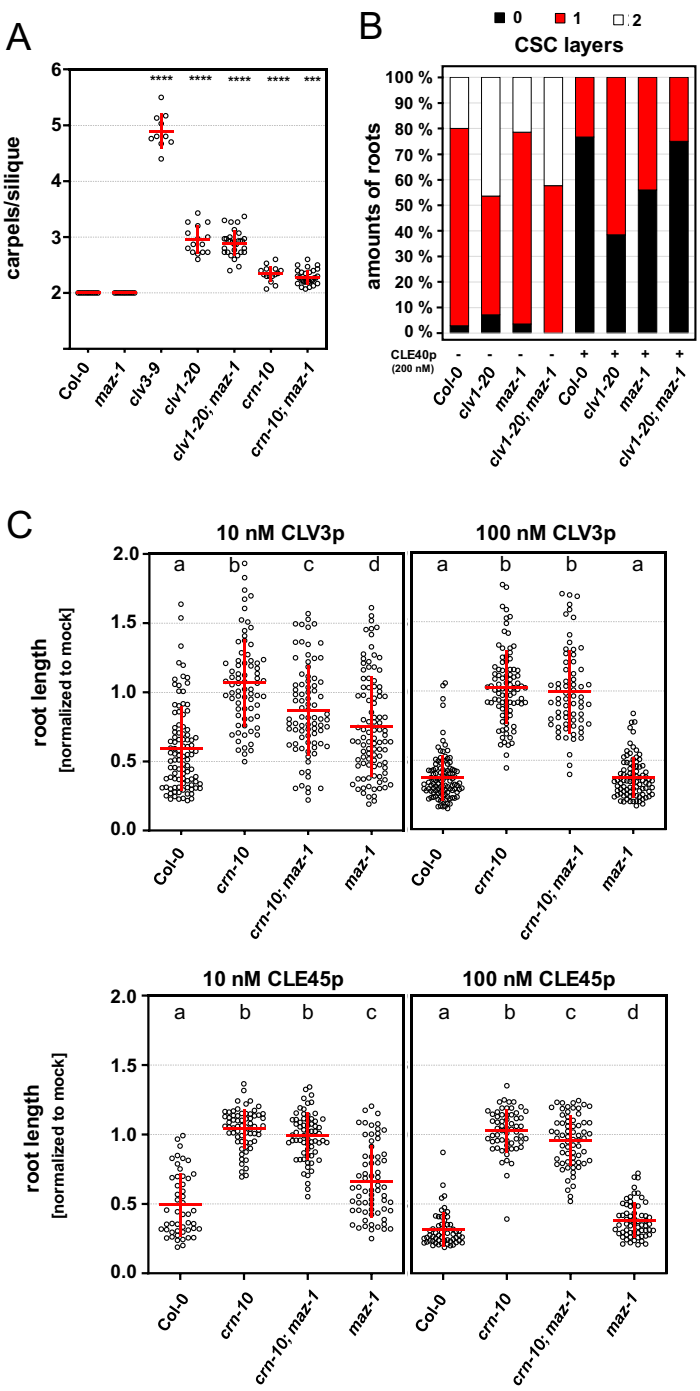

Figure 6 *Maz-1* mutants show no increased carpel number but are partially resistant against CLE peptide treatment.

A Mean carpel number per silique of indicated genotypes monitored in 6 – 8 weeks old plants grown under long day conditions. For each genotype 10 – 30 plants were analyzed by counting the carpels of 15 – 30 siliques per plant. The average carpel numbers for each plant are plotted. P-values calculated by ANOVA and Dunnett´s post hoc test with *** for $p \leq 0.001$, and **** for $p \leq 0.0001$. Sample mean and SD displayed in red. **B** CSC layers of indicated mutants quantified after mPS-PI staining of seedlings 5 DAG grown on ½ MS agar plates with and without 200 nM CLE40 peptide. **C** Root length of different genotypes 10 DAG grown on ½ MS agar plates supplemented with CLV3p or CLE45p at 10 nM and 100 nM, respectively. Data are normalized to the mean of the corresponding genotype grown without peptide. Statistical groups were assigned after calculating p-values by ANOVA and Dunnett´s post hoc test (differential grouping from $p \leq 0.05$). Sample mean and SD displayed.

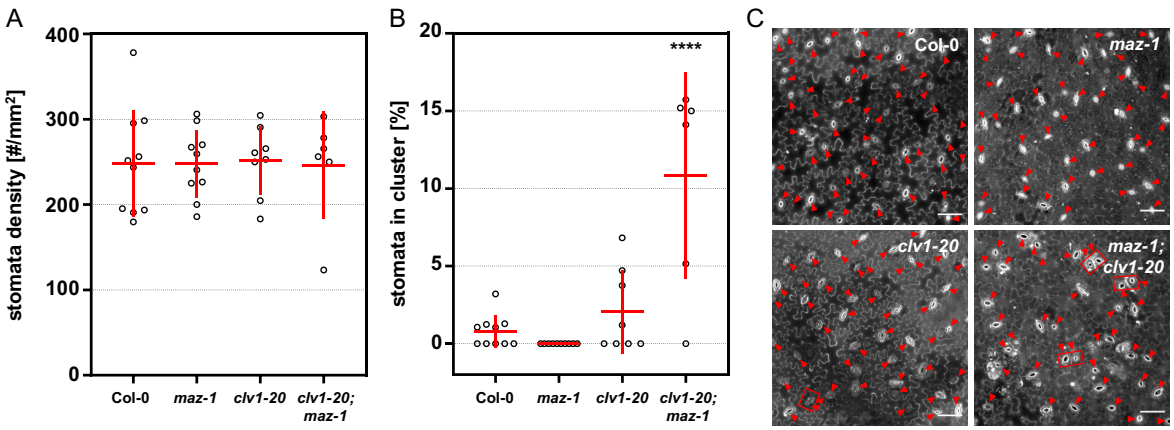

Figure 7 *Clv1-20;maz-1* double mutants display significantly increased stomata cluster rates.

A Stomatal density and **B** cluster rate were accessed from true leaves of indicated genotypes. Each plotted data point represents the mean value of 4 areas within one leaf of individual plants. Seedlings were grown on ½ MS agar plates. 14 DAG leaves were stained with PI to image abaxial epidermis cells. Significant differences in comparison to the Col-0 sample are indicated with **** for $p \leq 0.0001$, calculated by ANOVA and Dunnett´s post hoc test. Sample mean and SD displayed with red lines. **C** Representative images of the analyzed leaf epidermis areas counterstained with PI. Arrow heads mark stomata and boxes indicate clusters. Scale bars: 50 µm.

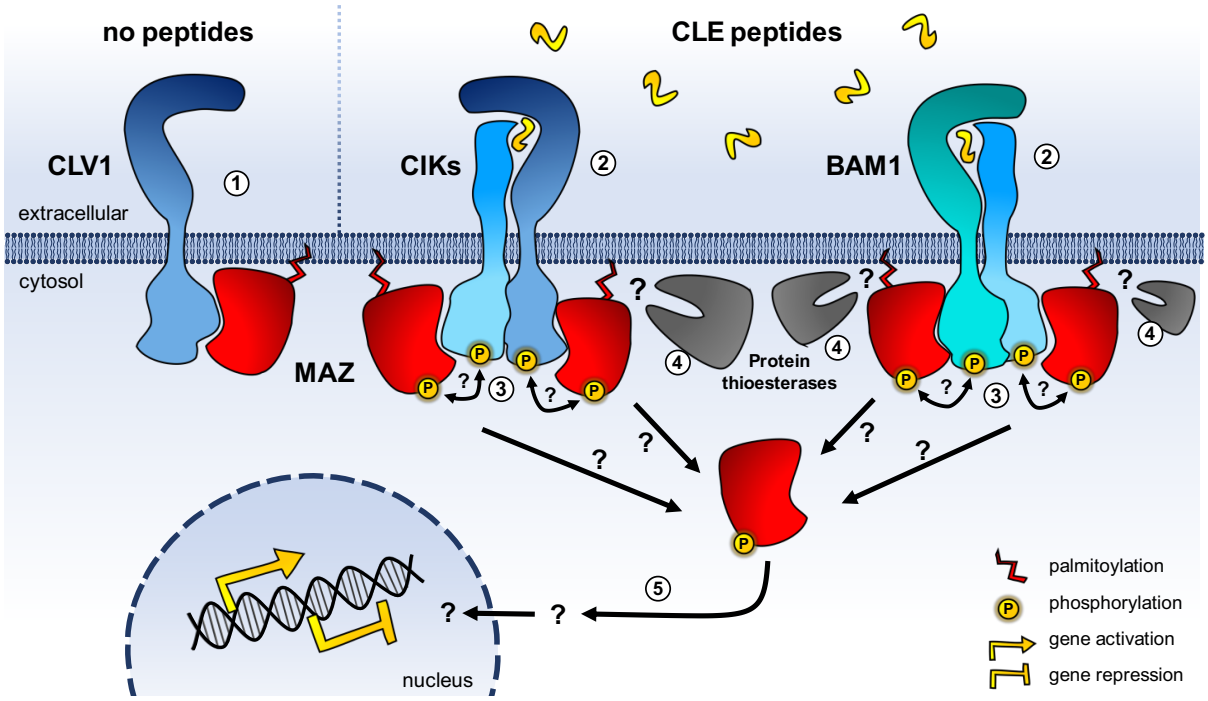

Figure 8 Model of MAZ as a signaling hub downstream of CLVf receptors.

In the absence of CLE peptides CLVf receptors and MAZ probably build preformed complexes (**1**). The CLE peptide perception by cognate CLVf receptors is aided by CIK co-receptors (**2**). Transphosphorylation between (co-)receptors and MAZ could transmit signal downstream (**3**). Protein thioesterases could catalyze release of activated MAZ from the PM by removing palmitoylation (**4**). Activated MAZ in the cytosol could mediate signal transduction to the nucleus (**5**).